NONLINEAR ULTRASONIC MEASUREMENT ON COLD ROLLED AND SENSITIZED 304 AUSTENITIC STAINLESS STEEL

A Thesis
Presented to
The Academic Faculty

by

Timm Geibel

In Partial Fulfillment
of the Requirements for the Degree
Master of Science in Engineering Science and Mechanics in the
School of Civil and Environmental Engineering

Georgia Institute of Technology
December 2017

NONLINEAR ULTRASONIC MEASUREMENT ON COLD ROLLED AND SENSITIZED 304 AUSTENITIC STAINLESS STEEL

Approved by:

Georgia Institute of Technology,
Committee Chair
School of Civil and Environmental
Engineering
Georgia Institute of Technology

Professor Laurence J. Jacobs, Advisor
School of Civil and Environmental
Engineering
Georgia Institute of Technology

Dr. Jin-Yeon Kim
School of Civil and Environmental
Engineering
Georgia Institute of Technology

Professor Jianmin Qu
G.W. Woodruff School of Mechanical
Engineering
Georgia Institute of Technology

Date Approved: August 14, 2017

ACKNOWLEDGEMENTS

First of all, I want to thank Professor Laurence Jacobs for making this research possible in his laboratory and working under his supervision. Your advice was always helpful and you always motivated me, even if the results were not as we expected them, to start over again and get back on track. Thank you for your patience with this work and for being more than a research adviser.

Special thanks to Dr. Kim, for all the help you gave me, all the experience you shared with me and all the good times we had that were not work related. You were always available when I was stuck in progress and with your advice and leadership, this work finally was made possible.

Dr. Joe Wall, thank you for trusting me with this research and helping me for preparing for the QNDE conference.

Thank you, Professor Preet Singh, for letting me use your lab equipment and always being helpful, but also sharing your experience on sensitization and material science.

Special thanks to Professor Michael Hanss and Dennis Schurr for selecting me to be part of this amazing program, always staying in contact throughout this special year and being there for us with advice and help at any time.

I want to thank the DAAD for supporting me financially throughout this year and the founding provided by EPRI that made this research possible.

Andrew Udell and Blake Blankini of the Environmental Department machine shop, Steven Sheffield and Louis Boulanger of the Montgomery machining hall, thanks to all of you for preparing my specimens and finding the right solutions for the processing steps.

I want to thank my lab mates, David Torello, for all the help and advice you gave me on the Rayleigh setup and the sport moments we shared, Gun Kim, for the late shifts we spend together in the lab and the friendship, Bryan Fuchs and Katie Scott, for an amazing QNDE conference and your knowledge and experience.

Special thanks to Miralem Saljanin and Steffen Maier, the students I started this journey with together, for all the trips we made, all the laughs we had and all the time we spend together in and outside of the lab.

Last but not least, I want to thank my family. I could have never achieved anything without them and their support in my life. Despite the distance and time shift, you were always there for me when I needed you and always inspired me and got me back on track, even in the saddest situations.

Thank you Andreas Geibel, dad, for never giving up on me, for always being there for me and for everything you have done. I would not be the person I am today and at this point of my life, without you.

TABLE OF CONTENTS

LIST OF TABLES

LIST OF FIGURES

LIST OF SYMBOLS OR ABBREVIATIONS

∂	partial derivative operator
δ	variational operator
β	acoustic nonlinearity parameter
δ_{ij}	Kronecker delta
ϵ_{ij}	strain tensor
θ	angle between surface and wave
λ	wavelength or first Lamé constant
κ	material constant
μ	second Lamé constant
ν	Poisson's ratio
π	mathematical constant
ρ	mass density
σ_{ij}	stress tensor
τ_{ij}	shear stress tensor
ϕ	number density or interpolation function
ω	angular frequency
Δ	Laplace operator
Ω	domain or region
c	wave velocity
c_R	Rayleigh wave speed
c_s	shear wave speed
c_L	longitudinal wave speed
d_{ij}	Euclidean distance matrix

e	exponential function
f	frequency
f_i	body force per mass vector
i	imaginary unit
k	wave number
n_i	normal vector
t	time or random vector
t_i	traction vector
u	displacement along first coordinate axis
u_i	displacement vector
x	first coordinate axis
y	second coordinate axis
z	third coordinate axis
x	thickness
x_i	i^{th} axis or direction in coordinate system
A	amplitude or Area
A_1	first harmonic wave amplitude
A_2	second harmonic wave amplitude
C_{ijkl}	higher order stiffness tensor
D_{ijkl}	higher order stiffness tensor
E	Young's modulus of elasticity or Larganian/ Green tensor
F_i	force vector
I	identity tensor
N	number of precipitates
P	non symmetrical tensor
S	surface or uniform grid size
U	internal work or approximated displacement

V	volume
W	external work

max	maximum
min	minimum
nm	nanometer
var	variance
EPR	Electrochemical potentiodynamic reactivation
IGSCC	Intergranular stress corrosion cracking
MS	microstructure
SS	Stainless Steel

SUMMARY

Austenitic stainless steels have a wide range of applications in the energy industry due to their high temperature performance and high corrosion resistance. Type 304 SS, is a widely used stainless steel, but is susceptible to sensitization, the formation of chromium carbide precipitates along the grain boundaries, causing chromium depletion when exposed to a certain temperature, ultimately leading to intergranular stress corrosion cracking (IGSCC). Sensitization preferably tends to occur in the heat affected zone (HAZ) of welds where heat is induced for a certain amount of time during welding. IGSCC is a main cause of the cracking in boiling water reactor piping systems and therefore is of great concern.

Nonlinear ultrasound is a nondestructive evaluation method measuring the change of harmonic frequencies over propagation distance quantified by the nonlinearity parameter, β. The research evaluates the changes of microstructure caused by cold work (cold rolling) using two nonlinear ultrasound methods, Rayleigh and longitudinal waves. Moreover it shows the sensitivity of nonlinear ultrasound to sensitization and combines sensitization and cold rolling, then is compared with previous work [20] [6] [17] that investigated just the isolated effect of sensitization, or cold work. The results show that (1) cold work causes significant variations in the nonlinearity parameter which can be attributed to the formation of dislocations and twins as a consequence of the plastic deformation and phase transformation and that (2) cold work has large influences on the sensitization behavior of 304 SS.

CHAPTER I

INTRODUCTION

1.1 Motivation and Objective

Austenitic stainless steels have a wide range of applications in the energy industry due to their high temperature performance and high corrosion resistance. Type 304 SS, is a widely used stainless steel, but this material is susceptible to sensitization, a phenomena where the material becomes sensitive to stress corrosion cracking. The formation of chromium carbide precipitates along the grain boundaries, causes chromium depletion when exposed to a certain temperature, ultimately leading to inter-granular stress corrosion cracking (IGSCC).

Sensitization tends to occur in the heat affected zone (HAZ), which can be seen in Figure 1 that shows the weld connecting two parent materials. The HAZ of welds is a zone where heat is induced for a certain amount of time during welding and its material properties are modified by the temperature influence. This is of great concern in nuclear power plants since the sensitization and associated IGSCC is a main cause of the cracking in boiling water reactor piping systems, but also of great importance wherever welds are used, as in constructions or the mechanical engineering sector in general. Sensitization of austenitic stainless steel occurs in the temperature range of 450°C to 850°C and therefore is also very important since austenitic steels are used at that temperature in many cases. The danger of IGSCC is the spreading of microcracks, which will lead to macrocracks and in the worst case to failure of the component, causing expensive changes or complete replacement.

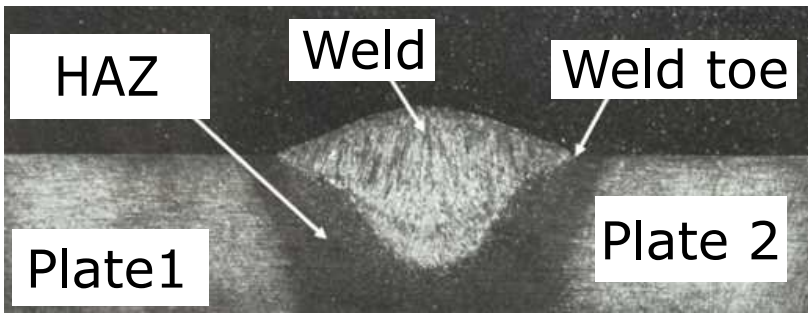

Figure 1: Cross section of a weld showing the Heat Affected Zone (HAZ) [13]

To avoid this, quantitative nondestructive evaluation (NDE) can be used to detect cracks before they result in fatal errors of the components. To this date, Rayleigh wave [5][6], longitudinal wave [20] and electrochemical [17] measurement methods were used on sensitized 304 SS specimens and showed the sensitivity and importance on chromium precipitation at the grain boundaries. Other research [11] [16] also demonstrated the sensitivity of longitudinal waves on thermical treated ferritic steel and reactor pressure vessel steel.

The objective of this research is two-fold:
First, the research evaluates the changes of microstructure caused by cold work (cold rolling) using nonlinear ultrasound (Rayleigh waves) and longitudinal waves and show the sensitivity and potential of nonlinear ultrasound measurement methods.
Second, the effect of prior cold work on the sensitization behavior of 304 SS is investigated using nonlinear ultrasound and then compared with previous work of Doerr [6], that investigated just the effect of sensitization, the experiments and results of A. Viswanath et al. [20], who investigated the effect of cold work on 304 SS and R. Singh et al. [17], who used electrochemical potentiokinetic reactivation (EPR) to show the effect of cold work on sensitized 304 SS specimens. This research also should clarify the question if cold work (cold rolling) helps strengthen the 304 SS and slows down the sensitization process, or even worse, supports it.

1.2 Structure of thesis

This thesis is organized as follows. Chapter 1 gives an overview about the motivation and objectives of this work, as well as the general structure. Chapter 2 is focusing on deforming process of cold working and cold rolling, additionally giving information about de- and sensitization in general and the annealing process. Chapter 3 informs about wave propagation and wave equations in general, then more detailed about surface Rayleigh waves and longitudinal waves. Moreover it derives the nonlinearity equations, finally leading to nonlinearity parameter, β. Chapter 4 describes previous works and studies made on sensitization and cold work on 304 SS to make comparisons to the measurement results of this work. Chapter 5 shows how the specimens used for this research were prepared. The different procedures and apertures of Rayleigh and longitudinal wave measurements, but also the EPR test are described in chapter 6. Chapter 7 presents the experimental results and compares them to previous work. The final chapter 8 provides conclusion and summary of the results, additionally gives and outlook and recommendation on future work and problems.

CHAPTER II

COLD WORK, SENSITIZATION AND ANNEALING OF STAINLESS STEEL

2.1 Cold work

In most cases metals are post-processed from their original shapes to, for example the desired shape, length or strength. There are many different kind of forming processes in the mechanical engineering sector, such as hardening, heating and bending, which have different effects on the grid structure and a result of that is changing the material constants and properties.

This section is focusing on work hardening, also known as cold working, especially cold rolling (2.1.1), a process where a metal plate is pushed through two or more combined mills to reduce the thickness, but also on desensitization and sensitization (2.2), which are effects occurring when heat is induced to metal for a certain amount of time at a certain temperature.

Cold working is a plastic deformation process. The process is called 'cold' work because the reshaping is done at temperatures below the metal's recrystallization point and most commonly used for steel and aluminum. Due to the change in the crystalline structure, the space for movement of those crystals is reduced, making the material more resistant to further deformation. This is underlining the advantage of cold rolling, combined with one of the disadvantages. The material is strengthened as seen in the increased tensile strength and hardness, but the ductility is decreased. Another advantage is the surface finish of cold rolled material. Even though a lot of stress is applied to the material, the surface ususally (if applied correctly) stays the same, or even gets better. A cold rolled specimen is for example susceptible to cracks,

if bend or further reformed with other procedures. There are different types of cold working methods that can be used to deform a specimen and are listed in table 1.

Table 1: Different cold working methods

Rolling	Bending	Shearing	Drawing
Extrusion	Angle bending	Blanking	Tube drawing
Coining	Roll forming	Slitting	Metal Spinning
Forging	Flanging	Lancing	Embossing

2.1.1 Cold rolling

This section focuses on cold rolling, a cold hardening process that is most commonly used in the power generation industry. It is also the stress inducing procedure that was investigated on in this thesis to compare the effect of cold rolling on the non-linearity parameter, β, and additionally sensitized 304 SS specimen.

During the cold rolling process a plate, or specimen with a certain thickness is passing through two (or more) rolling mills and the thickness is reduced to the required amount (see Figure 2).

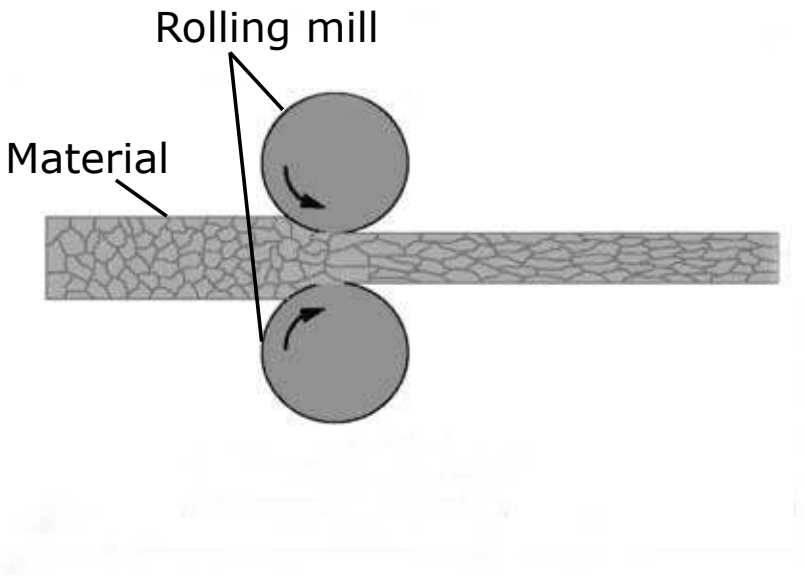

Figure 2: Cross section of a (cold) rolling mill [14]

Cold rolling has many advantages:

- Done at room temperature ⇒ no oxidation on surface
- highly suitable for mass production and automatisation processes
- excellent surface finish (if mills are in good condition) ⇒ eliminates subsequent machining
- good accuracy
- thin sheets can be produced
- not heat treatable specimen can still be improved by cold rolling

The material is plastically deformed and cannot return to the original thickness. Even though the material is reduced in thickness, it expands fractional after removing the stress. This effect is well known in material science as "spring back" and comparable to the stress strain curves of metals.

Cold rolling reduces the thickness of thin plates (dimension of 0.2 - 4 mm) to increase their strength. In this work the specimen had a thickness of 15 mm, so they fulfill the requirements of the Rayleigh wave measurement, which will be discussed in chapter 3.4.

2.2 Sensitization

The effect of sensitization occurs in materials such as stainless steels, when heat between 450°C to 850°C is induced for a certain amount of time, but also during the welding process in the HAZ (see Figure 1 in chapter 1). As a result of that intergranular stress corrosion cracking (IGSCC) can occur, which is highly undesirable, since it weakens the material and can lead to its failure.

The precipitation and depletion of chromium along the grain boundaries is sensitization. This effect depends on many different factors such as temperature and time. Some forming processes also influence sensitization and may accelerate the sensitization rate. Singh et al. [17] show that for example cold rolling has an effect on the sensitization, because the rolling process is creating space between the grains, leaving holes where the chromium solutes can gather. This effect will be investigated with longitudinal and Rayleigh wave measurements in chapter 7 and compared.

In figure 3 the process of sensitization on AISI 316 steel to different holding times, for example 700°C is presented. The precipitated chromium is visible as dark lines along the grain boundaries. Longer holding times with the same temperature causes increased precipitation and therefore is increasing the sensitization effect.

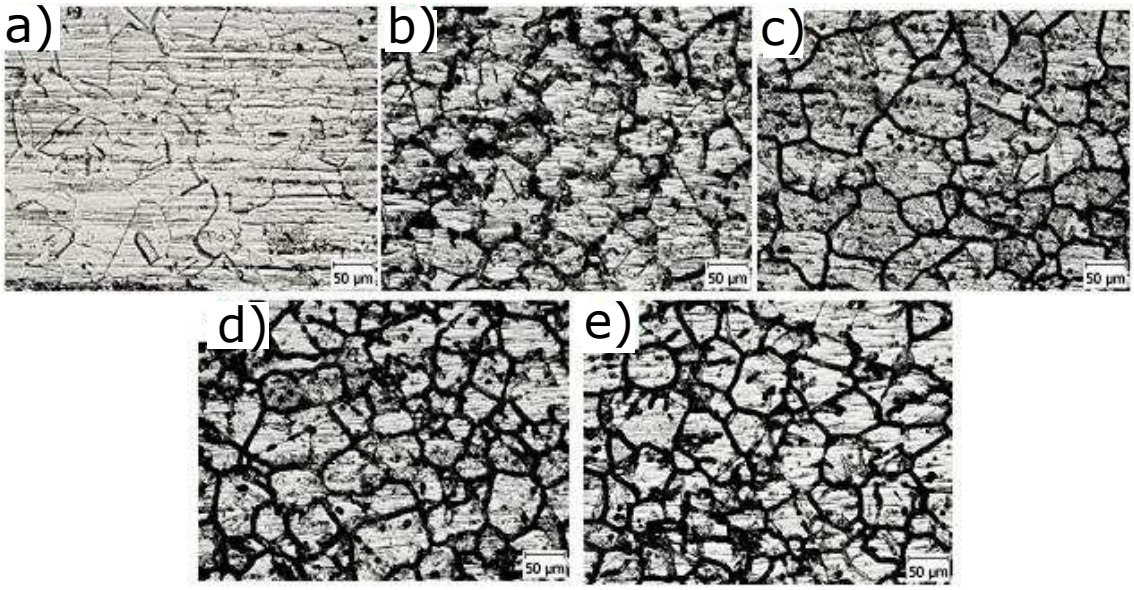

Figure 3: Micro-structure of AISI 316 specimens at different holding times at a temperature of 700°C for a) 15 min b) 30 min c) 60 min d) 300 min e) 600 min [10]

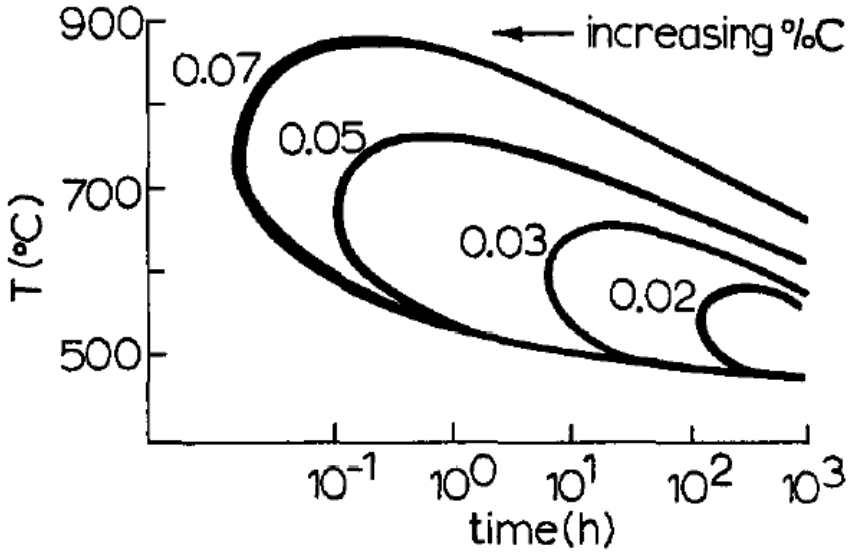

Figure 4: Effect of carbon content in a material on sensitization [19]

Sensitization is a complex process and depends on different factors:

- Temperature and holding time of the specimen as it can be seen in figure 4
- Carbon content of the material. This effect can be seen in figure 4 with decreasing carbon content, the sensitization temperature decreases, while the sensitization time increases
- desensitization effect; self healing of the material after long holding times
- grain size, as well as the grain orientation
- cold work
- steel phases/ material composition

2.3 Desensitization

Desensitization is another effect that can occur when steel is held for a certain amount of time in a temperature range between 450°C to 850°C. It basically is the self healing of the material , after sensitization has occurred. Therefore the same kind of factors also have an impact on the desensitization, as described previously in chapter 2.2.

As seen in figure 5 the degree of sensitization (DOS), a gradient that gives information about how much sensitization is present in the material, is increasing for all measured strains to a maximum. But, after approximately 10h, drops nearly to zero. With this work Beltran et al. [3] shows the capability of 304 to recover itself and (nearly) desensitize completely. This underlines the impact of holding time and temperature on sensitization.

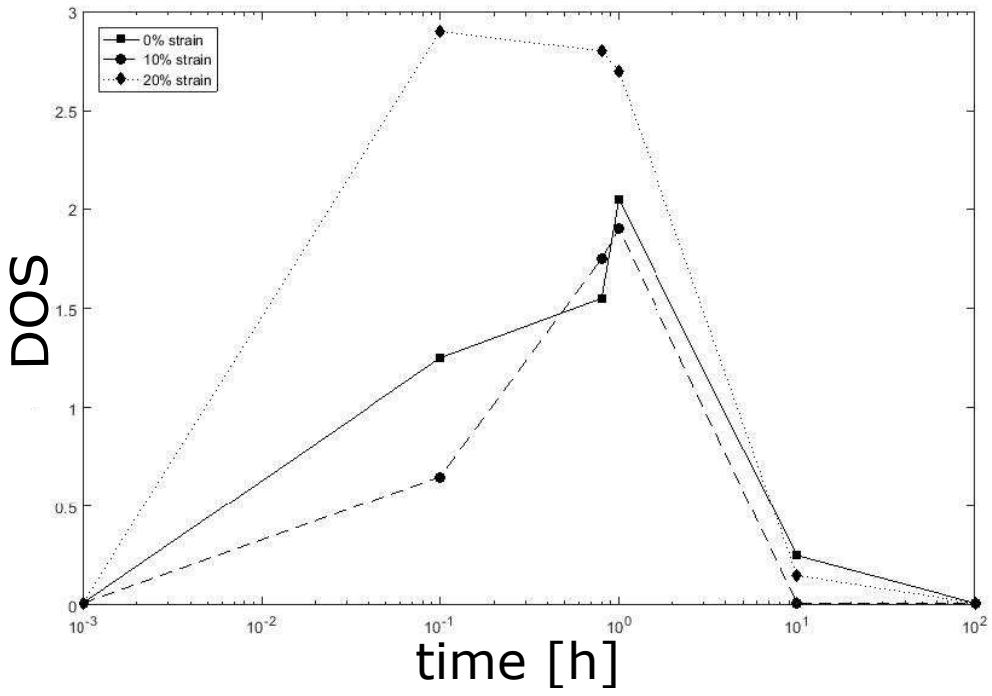

Figure 5: Comparison of EPR-DOS (sensitization) curves for type 304 stainless steel deformed at strains shown and hold at 625°C for certain time [3]

2.4 Annealing of Stainless Steel

Another heat treatment that is used on the 304 specimen is annealing. In general it is a procedure that can be used for metal, but also for copper and silver. The effect of it differs and depends on the material. In metallurgy there are different phases like austenitic, martensitic or ferritic steel. The objective of annealing is increasing its ductility and reducing the hardness, so the material gets more workable. The material is heatend up above its recrystallization temperature, held at that temperature for a certain time and then cooled down, either quenched with water or oil (fast cooling/shock), or slowly at room temperature.

During that process the atoms migrate, decreasing the number of dislocations and is often used to remove stress in the material. Nonetheless, annealing depends on temperature and the crystaline phase. Austenitic stainless steel, such as 304 SS, is

softened when annealed in the temperature range of 1050°C to 1120°C, whereas this heat treatment would harden a martensitic steel.

In this study annealing is used to bring the specimen to the same level and remove previous stress, that could have been induced to the material during production, for example cold or hot work. Doerr [5] [6] shows in his thesis that unannealed specimens follow complicated behavior when sensitized, whereas pre annealing a specimen creates a constant microstructure, enabling comparison of sensitization results.

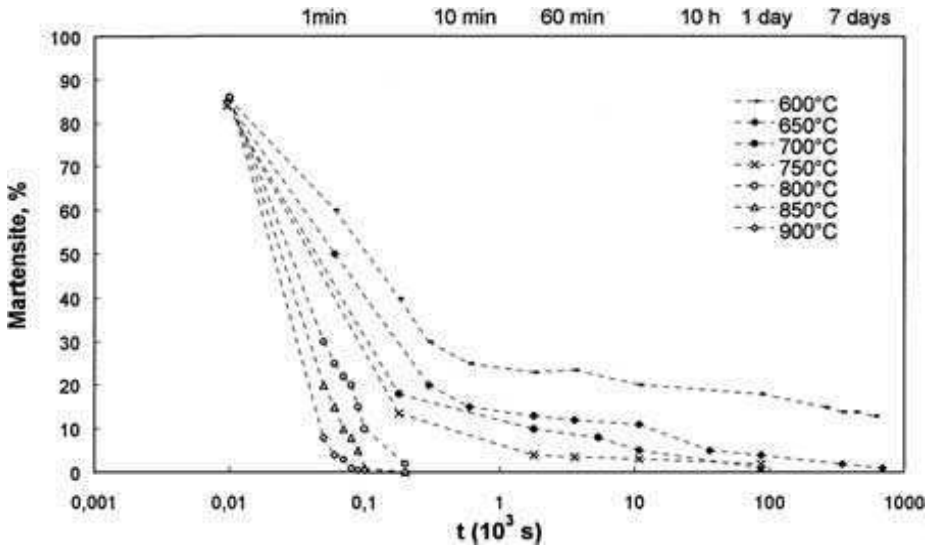

Figure 6: Effect of time and temperature during annealing on martensite induced 304 SS by cold work [15]

In figure 6 the effect of annealing on cold worked 304 SS is shown. Putting cold worked specimen in the furnace at a temperature of 900° for an hour is transforming the martensite completely and bringing it back to zero. This effect will be investigated on in chapter 7.4.

CHAPTER III

WAVE PROPAGATION IN MATERIALS

The Rayleigh wave measurements, as well as the longitudinal measurements display the changes of the nonlinearity paramater, β. With these nonlinearity parameter changes in the material, effects as sensitization, cold work, annealing and IGSCC, can be detected. β is defined as

$$\beta = \frac{8\,A_2}{x\,k^2\,A_1^2} \propto \frac{A_2}{A_1^2} \tag{1}$$

and proportional to the ratio A_2/A_1^2 traveling through or on the surface of the material. In Eq. 1, A_1 and A_2 are the amplitudes of the fundamental and second harmonic waves. In the longitudinal wave case the thickness x, is set to be constant. In this chapter an overview on the principles of wave propagation in elastic solids is shown and discusses the theoretical basis on the explanations of Achenbach [1] and Graff [7]. The plane wave propagation leads to the Rayleigh surface wave, as well as to the longitudinal wave and the nonlinearity parameter, β will be derived in the following chapter.

3.1 Equation of Motion

To derive equation (1) the general form of the linearized theory leads to

$$\int_S t\,\mathrm{d}A + \int_V \rho f\,\mathrm{d}V = \int_V \rho\ddot{u}\,\mathrm{d}V \tag{2}$$

where V (Volume) and S (Surface) is a close region with S as boundary and area A, with the second derivative of the displacement u and the body force per unit mass f and t. This leads to the "Cauchy-Stress formula" with stress tensor τ and orientation n.

$$t_l = \tau_{kl}\,n_k \tag{3}$$

By substituting equation (3) into equation (2) it can be rewritten as

$$\int_S \tau_{kl}\, n_k \,\mathrm{d}A + \int \rho\, f_l \,\mathrm{d}V = \int_V \rho\, \ddot{u}_l \,\mathrm{d}V. \tag{4}$$

With the the Gauss theorem this equation can be rewritten as

$$\int_V (\tau_{kl,k} + \rho\, f_l - \rho\, \ddot{u}_l) \,\mathrm{d}V = 0. \tag{5}$$

V is an arbitrary part of the material and the integrand is continuous so that

$$\tau_{kl,k} + \rho\, f_l = \rho\, \ddot{u}_l \tag{6}$$

and defines Cauchy's first law of motion.

In general the relation betwenn stress tensor τ_{ij} and strain tensor $\varepsilon_{\mathrm{kl}}$ is defined by

$$\tau_{ij} = C_{ijkl}\, \varepsilon_{kl} \tag{7}$$

and the elastic stiffness tensor $\mathrm{C_{ijkl}}$, which are constants and defined as

$$C_{ijkl} = C_{jikl} = C_{klij} = C_{ijlk}. \tag{8}$$

Using Hook's law equation (7) is transfromed to

$$\tau_{ij} = \lambda\, \varepsilon_{kk}\, \delta_{ij} + 2\, \mu\, \varepsilon_{ij}. \tag{9}$$

The two elastic constants λ and μ are known as the Lamé constants and are defined as

$$\lambda = \frac{E\,\nu}{(1+\nu)(1-2\,\nu)} \qquad\qquad \mu = \frac{E}{2(1+\nu)} \tag{10}$$

with the Young's modulus E and the Poisson's ratio ν. With the stress equation of motion (6), equation (9) and the strain displacement relation (11)

$$\varepsilon_{ij} = \frac{1}{2}(u_{ij} + u_{j,i}) \tag{11}$$

we obtain the displacement equation of motion

$$\mu\, u_{i,jj} + (\lambda + \mu) u_{j,ji} + \rho\, f_i = \rho\, \ddot{u}_i. \tag{12}$$

This can be rewritten into vector notation

$$\mu \nabla^2 u + (\lambda + \mu)\nabla\nabla u = \rho\ddot{u}. \tag{13}$$

If the body forces and stress tensors depend on one variable and one direction, for example x_1 the equation of motion is

$$(\lambda + 2\mu)u_{1,11} + \rho f_1 = \rho \ddot{u_1} \tag{14}$$

longitudinal stress. Equation (13) leads to the propagation velocity of longitudinal waves and is parallel to the direction of propagation

$$c = c_L = \sqrt{\left(\frac{\lambda + 2\mu}{\rho}\right)}, \tag{15}$$

as well as to the wave velocity of rotational waves, so called shear waves (S-wave)

$$c = c_S = \sqrt{\frac{\mu}{\rho}}. \tag{16}$$

3.2 Linear Wave Propagation

3.2.1 Plane shear and longitudinal waves

The described longitudinal and shear waves are so called plane waves. Plane waves are waves where the wavefront consists of infinite parallel waves propagating through a material.

A plane displacement wave propagating with velocity c in a direction defined by vector p can be displayed as

$$u = f\,(x\,p - c\,t)d, \tag{17}$$

where d and p are normal vectors defining the direction of the wave propagation, the position x and time t. With equation (13) and (17) the shear and longitudinal wave velocities (equation (15),(16)) were derived.

Equation (17) can be extended to the time harmonic plane wave displacement

$$u = A\,d\,e^{i\,k(x\,p - c\,t)}, \tag{18}$$

where A is the Amplitude and wavenumber k, defined by

$$k = \frac{2\,\pi}{\Lambda}. \tag{19}$$

Equation (18) is a special case of equation (17).

3.3 Reflection of longitudinal and shear waves

An important part of wave propagation in materials is the reflection of those waves at the boundaries, for example the transition between two materials. Achenbach [1] is explaining this phenomenon in his book. The displacement for a longitudinal or a shear wave is defined by

$$u^{(n)} = A_n\, d^{(n)}\, e^{(i\,\eta_n)} \tag{20}$$

where the wave propagates in x_1-x_2 direction. The index n describes the different types of waves that can occur when a wave is reflected. Parameter η can be defined as

$$\vec{\eta_n} = k_n\,(x_1\,p_1^{(n)} + x_2\,p_2^{(n)} - c_n\,t). \tag{21}$$

Figure 7 displays the incoming P-wave and the reflection cases that can occur. Depending on the incoming angle θ_0, the angle of the reflection waves differ and change the reflected waves to shear waves.

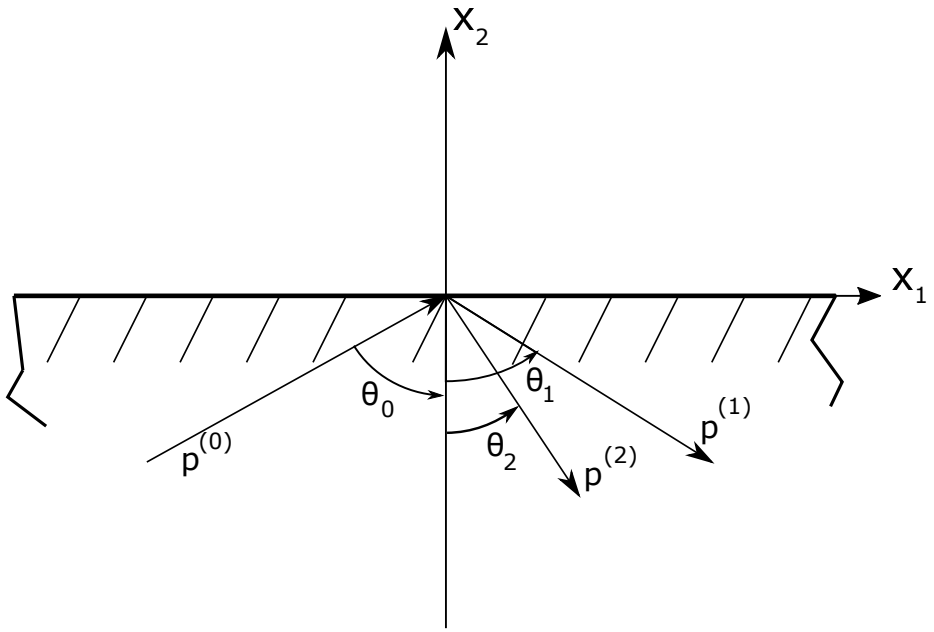

Figure 7: Incoming incident P/S wave and reflection on a free material surface

With the material constant κ

$$\kappa = \sqrt{\frac{2\,(1-\nu)}{1-2\,\nu}}, \tag{22}$$

the simple relations for the wave number and angle are

$$k_1 = k_0 \tag{23}$$

$$k_2/k_0 = c_L/c_T = \kappa \tag{24}$$

$$\theta_1 = \theta_0 \tag{25}$$

$$sin\theta_2 = \kappa^{-1} sin\theta_0 \tag{26}$$

and lead to the wave velocity on the surface at $x_2 = 0$

$$c = \omega/k = c_L/sin\theta_0. \tag{27}$$

If the incident angle of a shear wave is in a critical area, the reflected wave will be a shear wave that travels on the surface of the material, so called Rayleigh wave. This

Rayleigh wave appears when the critical angle θ_C is

$$\theta_C = arcsin\frac{c_S}{c_L}, \tag{28}$$

where c_S is the shear wave velocity and c_L the incident wave velocity.

3.4 Rayleigh Surface Waves

Rayleigh surface wave are shear waves travelling along the material surface, because the incident wave hits the material surface with the critical angle θ_c (equation (28). The amplitude of a Rayleigh wave decreases with increasing material depth and is approximatly one wavelength above surface.

With Rayleigh waves IGSCC can be detected and a long distance (depending on the material) can be measured. Figure 9 shows the propagation of a Rayleigh wave in x_1 direction. The wave propagates over a certain distance and excites the particles to move on an elliptical path.

Rayleigh waves are often used in non-destructive testing to detect defects.

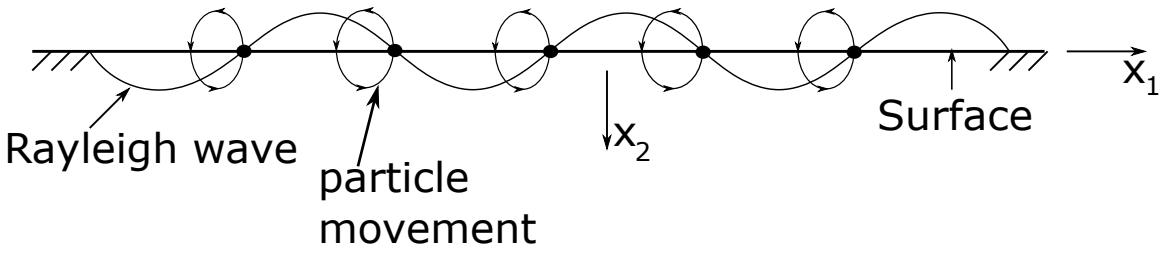

Figure 8: Rayleigh wave propagating on material surface

Rayleigh surface waves decay with distance from the surface exponentially. In a two dimensional case, where the wave propagates in x_14 direction and the material thickness is in x_2 (u_3=0, displacement in x_3), the displacement components are

$$u_1 = A\, e^{-bx_2} e^{ik(x_1 - c_R\, t)} \tag{29}$$

$$u_2 = A\, e^{-bx_2} e^{ik(x_2 - c_R\, t)}, \tag{30}$$

where c_R is the phase velocity of the Rayleigh wave. The real part of parameter b has to be positive to ensure the decrease of displacement in x_2 direction. By putting equation (28)(29) into the equation of motion (13) a nontrivial equation of this system is obtained as

$$[c_L^2\, b^2 - (c_L^2 - c_R^2)k^2][c_T^2\, b^2 - (c_T^2 - c_R^2)k^2] = 0. \tag{31}$$

With equation (31) the two constants

$$b_1 = k\sqrt{1 - \frac{c_R^2}{c_L^2}}, \qquad and \qquad b_2 = k\sqrt{1 - \frac{c_R^2}{c_T^2}} \tag{32}$$

are determined, which have are real and positive if $c_R < c_T < c_L$. With these equations the ratio of (B/A) can be written as

$$\left(\frac{B}{A}\right)_1 = -\frac{i\,k}{b_2} \qquad and \qquad \left(\frac{B}{A}\right)_2 = -\frac{b_1}{i\,k}. \tag{33}$$

These equations returned into equation(29)(28) leads to the general solution of the displacement

$$u_1 = [A_1\ e^{-b_1\, x_2} + A_2\ e^{-b_2\, x_2}]\, e^{ik(x_1 - c_R\, t)} \tag{34}$$

$$u_2 = [-\frac{b_1}{i\,k} A_1\ e^{-b_1\, x_2} + \frac{i\,k}{b_2} A_2\ e^{-b_2\, x_2}]\, e^{ik(x_1 - c_R\, t)} \tag{35}$$

For the nontrivial solution the coefficients A_1 and A_2 vanish, which leads to equation of the Rayleigh phase velocity

$$\left(2 - \frac{{c_R}^2}{{c_T}^2}\right)^2 - 4\sqrt{\left(1 - \frac{{c_R}^2}{{c_L}^2}\right)}\sqrt{\left(1 - \frac{{c_R}^2}{{c_T}^2}\right)}. \tag{36}$$

The Rayleigh phase velocity can be approximately calculated by

$$c_R \approx \frac{0.862 + 1.14\nu}{1 + \nu}\, c_T. \tag{37}$$

As already mentioned the displacement decreases exponentially in x_2 direction. Achenbach [1] shows that most of the Rayleigh wave energy is located betwee $x_2 = 0$ (Surface) and the $x_2 = \Lambda_R$, which is the wavelength.

3.5 Nonlinear Wave Propagation

The propagation of linear waves is an assumption made for idealistic, isotropic and homogeneous materials. Unfortunatly the behavior of material and therefore the propagation of ultrasonic waves differ from the linear assumption and due to that effect, the wave generates higher harmonic.

By measuring the amplitude of the harmonic, the non-dimensional nonlinearity parameter,β, informs about the stress-strain relation of the solid. With this parameter the behavior of materials can be investigated and the effect of, for example sensitization or cold work, can be displayed.

To derive the equation for β, the momentum balance equation of wave motion in solids is necessary. All following equations are out of "Nonlinear Acoustics"' by Hamilton and Blackstock [4]:

$$\rho \frac{\mathrm{d}\, u}{\mathrm{d}\, t} = \nabla\, \sigma, \tag{38}$$

where ρ is mass density, particle velocity $u = x - a$ and stress tensor σ. To connect the current and material description the deformation tensor

$$F = \frac{\partial\, x}{\partial\, a} = I + \frac{\partial\, U}{\partial\, a} = F_{ij} = \frac{\partial\, x_i}{\partial\, a_j}, \tag{39}$$

with identity tensor I, is necessary. The Lagrangian/Green tensor is given by

$$E = \frac{1}{2}(F^T\, F - I) \tag{40}$$

or,

$$E_{ij} = \frac{1}{2}\left(\frac{\partial U_i}{\partial\, a_j} + \frac{\partial U_j}{\partial a_i} + \frac{\partial U_k}{\partial a_i}\frac{\partial U_k}{\partial a_j}\right). \tag{41}$$

To transform equation(38) into Lagrangian coordinates, the non-symmetric tensor P defined as

$$P = \frac{\rho_0}{\rho}\, \sigma (F^{-1})^T, \tag{42}$$

also known as the Piola-Kirchhoff stress tensor. With these equations

$$\rho_0 \frac{\partial^2 U}{\partial t^2} = \nabla_a\, P \tag{43}$$

follows, where ∇_a is the gradient for the material coordinates, finally leading to a simplified form of P and σ

$$P = \rho_0 \, F \, \frac{\partial W}{\partial E} \qquad \Leftrightarrow \qquad \sigma = \rho \, F \, \frac{\partial W}{\partial E} \, F^T. \tag{44}$$

With the assumption for small strainsr the strain energy becomes

$$\rho_0 \, W = \frac{1}{2!} \, C_{ijkl} \, E_{ij} \, E_{kl} + \frac{1}{3!} \, C_{ijklmn} E_{ij} \, E_{kl} \, E_{mn} + ... \tag{45}$$

and combined with equation(43) leads to

$$P_{ij} = C_{ijkl} \frac{\partial \, U_k}{\partial a_l} + \frac{1}{2} \, M_{ijklmn} \frac{\partial U_k}{\partial a_l} \frac{\partial U_m}{\partial a_n} + \frac{1}{3} M_{ijklmn} \frac{\partial U_k}{\partial a_l} \frac{\partial U_m}{\partial a_n} \frac{\partial U_p}{\partial a_q} + ..., \tag{46}$$

where

$$M_{ijklmn} = C_{ijklmn} + C_{ijln} \delta_{km} + C_{jnkl} \delta_{im} + C_{jlmn} \delta ik. \tag{47}$$

Combining equation (43) and (46) leads to an equation of motion, without including viscosity, which is defined as

$$\rho_0 \frac{\partial^2 U_i}{\partial t^2} = \frac{\partial^2 U_k}{\partial a_j \partial a_l} \left(C_{ijkl} + M_{ijklmn} \frac{\partial U_m}{\partial a_n} + ... \right). \tag{48}$$

Kim et al. [9] describes a way to derive this equation of motion, finally leading to the nonlinear parameter, β. Equation (48) of a solid element, without body forces, is defined as

$$\rho \frac{\partial^2 u_i}{\partial t^2} = \frac{\partial \sigma_{ij}}{\partial X_j}, \tag{49}$$

with displacement tensor u_i. The stress tensor σ_{ij} in a nonlinear solid can generally be written as

$$\sigma_{ij} = \sigma_{ij}^0 + A_{ijkl} \frac{\partial u_k}{\partial X_l} + \frac{1}{2} \, A_{ijklmn} \frac{\partial u_k}{\partial X_l} \frac{\partial u_m}{\partial X_n} + ..., \tag{50}$$

where A_{ijklmn} are the Huang coefficients, related to the second and third elastic constants. By considering one dimensional wave propagation of a longitudinal wave, equation (49) and (50) transform to

$$\frac{\partial^2 u_1}{\partial t^2} = c^2 \frac{\partial^2 u_1}{\partial X_1^2} \left(1 + \beta \frac{\partial u_1}{\partial X_1} \right). \tag{51}$$

A time harmonic plane wave $A_1 cos(kX_1 - \omega t)$ traveling through a medium and the assumption that the nonlinearity is small, the solution for equation (50) is

$$\begin{aligned} u_1 &= -\frac{1}{8}\beta\, k^2\, A_1^2\, X_1 + A_1\, cos(kX_1 - \omega\, t) \\ &\quad + \frac{1}{8}\beta\, k^2\, A_1^2\, X_1\, cos[2(kX_1 - \omega\, t)]... \\ &= A_0 + a_1 cos(k\, X_1 - \omega\, t) + A_2 cos[2(kX_1 - \omega\, t)] + ... \end{aligned} \tag{52}$$

The nonlinearity parameter, β, is determined experimentally and depends on the first (A_1) and second harmonic (A_2) displacement signals, finally leading to equation

$$\beta = \frac{8\, A_2}{k^2\, X_1\, A_1^2}, \tag{53}$$

which is neglecting the effect of attenuation losses of the harmonics. This parameter displays the changes of the two harmonic amplitudes, giving information about the nonlinearity in the material.

3.5.1 Nonlinearity of Rayleigh surface waves

As already mentioned, Rayleigh waves are a combination of longitudinal and shear waves propagating on the surface of the material. However, the solution of equation (51) is only valid for one-dimensional longitudinal waves. Since the acoustic nonlinearity for shear waves is small compared to the longitudinal waves, it can be neglected and therefore the nonlinearity parameter for Rayleigh waves is derivable.

Hermann [8] is showing in his work how the nonlinearity parameter is defined. As a first step a Rayleigh wave is propagating in the positive x-direction, while z is pointing into the material, as it can be seen in figure 9.

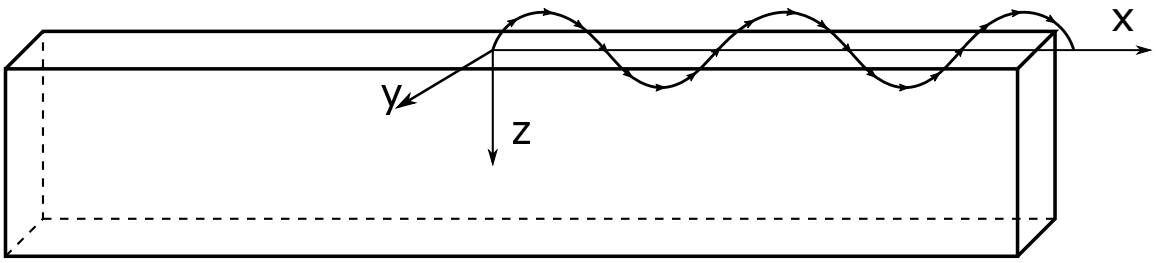

Figure 9: Rayleigh wave propagating in x-direction

As already mentioned Rayleigh waves are a superposition of shear and longitudinal waves and are propagating on the stress free surface, leading to the displacement components in x and z direction as

$$u_x = B_1 \left(e^{-pz} - \frac{2\,p\,s}{k_R^2 + s^2} e^{-sz} \right) e^{i(k_R x - \omega\, t)} \tag{54}$$

and

$$u_z = i\, B_1 \frac{p}{k_R} \left(e^{-pz} - \frac{2\,k_R^2}{k_R^2 + s^2} e^{-sz} \right) e^{i(k_R x - \omega\, t)}, \tag{55}$$

where $p^2 = k_R^2 - k_l^2$, $s^2 = k_R^2 - k_s^2$ and k_R, k_s, k_l are the wave numbers for Rayleigh, shear and longitudinal waves.

The second harmonic waves propagating a large distance in a nonlinear medium can be displayed as

$$u_x \approx B_2 \left(e^{-2pz} - \frac{2\,p\,s}{k_R^2 + s^2} e^{-2sz} \right) e^{i\,2(k_R x - \omega\, t)} \tag{56}$$

$$u_z \approx i\, B_2 \frac{p}{k_R} \left(e^{-2pz} - \frac{2\,k_R^2}{k_R^2 + s^2} e^{-2sz} \right) e^{i\,2(k_R x - \omega\, t)}. \tag{57}$$

As already mentioned the nonlinearity for a shear wave in an isotropic material can be neglected due to the symmetry of the elastic constants. Therefore the amplitudes of the first order harmonic of the longitudinal and the second harmonic of the Rayleigh wave can be related, so

$$B_2 = \frac{\beta\, k_l^2\, x\, B_1^2}{8} \tag{58}$$

finally leading to the nonlinearity parameter, β for nonlinear Rayleigh waves

$$\beta = \frac{8\, i\, \bar{u_z}(2\,\omega\, p)}{k_l^2\, x\, \bar{u_z^2}(\omega) k_R} \left(1 - \frac{2\,k_R^2}{k_R^2 + s^2} \right), \tag{59}$$

which is simplified to

$$\beta' = \frac{A_2}{x\, A_1^2} \propto \beta, \tag{60}$$

if the frequency is constant during the measurements. The nonlinearity parameter,β, is the key parameter in this research for the Rayleigh wave and longitudinal wave

measurements procedures. Changes in the material after putting stress or thermical changes can be displayed by the change of β. The measurement setups and specimen preparation are described in the following chapters.

CHAPTER IV

PREVIOUS MEASUREMENTS ON 304 STAINLESS STEEL AND RELATED STUDIES

Previous studies of Doerr [6], Viswanath et al. [20] and Singh et al. [17] investigated on the effect of sensitization on 304 SS, but also on the effect of sensitization on cold rolled 304 SS. They used different techniques and measurement setups to describe the behavior of the material. Their results and setup will be described briefly in the following chapter and in chapter 7 as a comparison to the results of this work.

4.1 Use of Rayleigh waves on sensitized 304 SS

Doerr [6] investigated on the effect of sensitization on 304 SS by using nonlinear Rayleigh waves. Different specimens were prepared equally and previously annealed in the same furnace. The specimen then were sensitized by putting them in a furnace at 675°C for different holding times.

Afterwards these specimens were surface grinded and hand polished with GRIT sand paper 2500 to enable the same surface condition. The results of the measurements can be seen in figure 10.

The nonlinearity parameter, β, undergoes a drastical increase after a holding time of 150 min and reaches it maximum at 250 min, where it remains even for longer holding times. At the maximum point the specimen are fully sensitized and no more chromium precipitates are formed. It is assumed that after a certain amount of time the self healing process described earlier, desensitization, would occur. It is also obvious that the begin of sensitization needs time, since β is nearly constant between 0-150 min.

Doerr [6] observed the increase of β by the larger size and number of precipitated chromium carbide, due to the longer holding times. This not only shows that sensitization has an effect on the nonlinearity parameter that can be related to the precipitation of chromium carbide, but also the sensitivity of Rayleigh wave measurements in general on heat treatment.

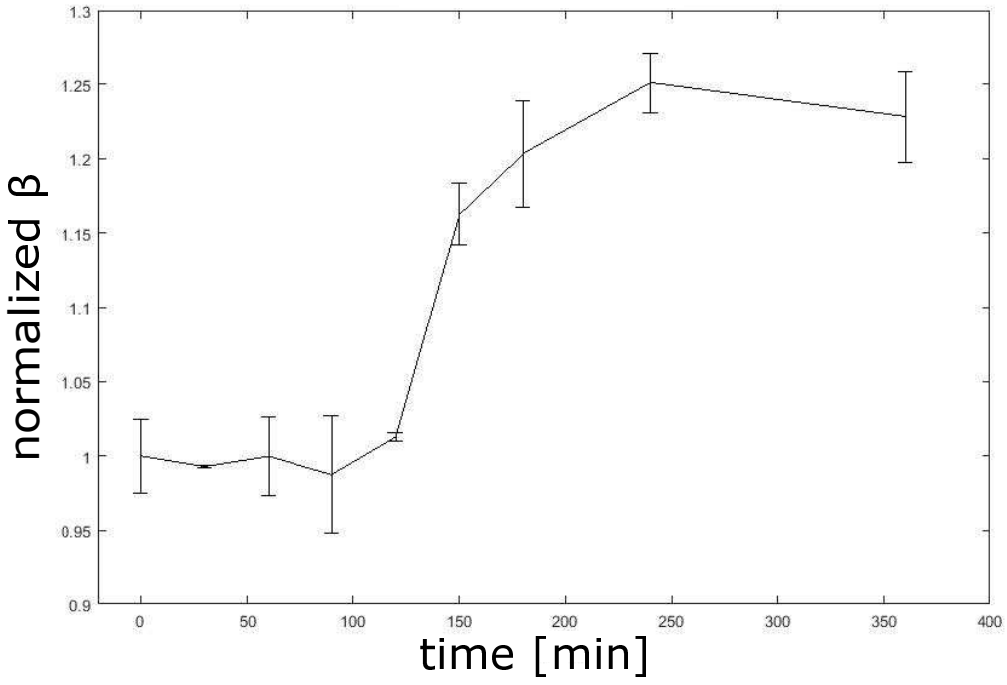

Figure 10: Nonlinearity parameter β over holding time of sensitized 304 SS specimen [5]

4.2 Longitudinal wave measurement on cold rolled stainless steel

In 'nondestructive assessment of tensile properties of cold worked AISI type 304 SS using nonlinear ultrasonic technique' Viswanath et al. [20] investigates the influence of cold rolling on 304 SS by measuring the nonlinarity parameter, β, using longitudinal waves.

Six specimen are prepared for the measurements and had an original thickness

of 5 mm. They were solution annealed at 1323 K, then cold rolled to reduce the thickness from 10% up to 47 % and measured. Furthermore X-Ray diffraction and scanning electron microscopy measurements were made too, but will not be further discussed in this thesis.

Figure 11 shows the results of the longitudinal measurement and the raise of β for different rolling percentages. It points out that β increases monotonically with increase of cold work and reaches it maximum at 47 %, where β is nearly 170 % higher compared to the not-rolled specimen. This increase is caused by the transformation of austenitic steel to α' martensite, as well as the formation of dislocations, formation of grains and dislocation of double walls.

Therefore longitudinal wave measurement is sensitive to cold rolling in 304 SS and can be measured by β.

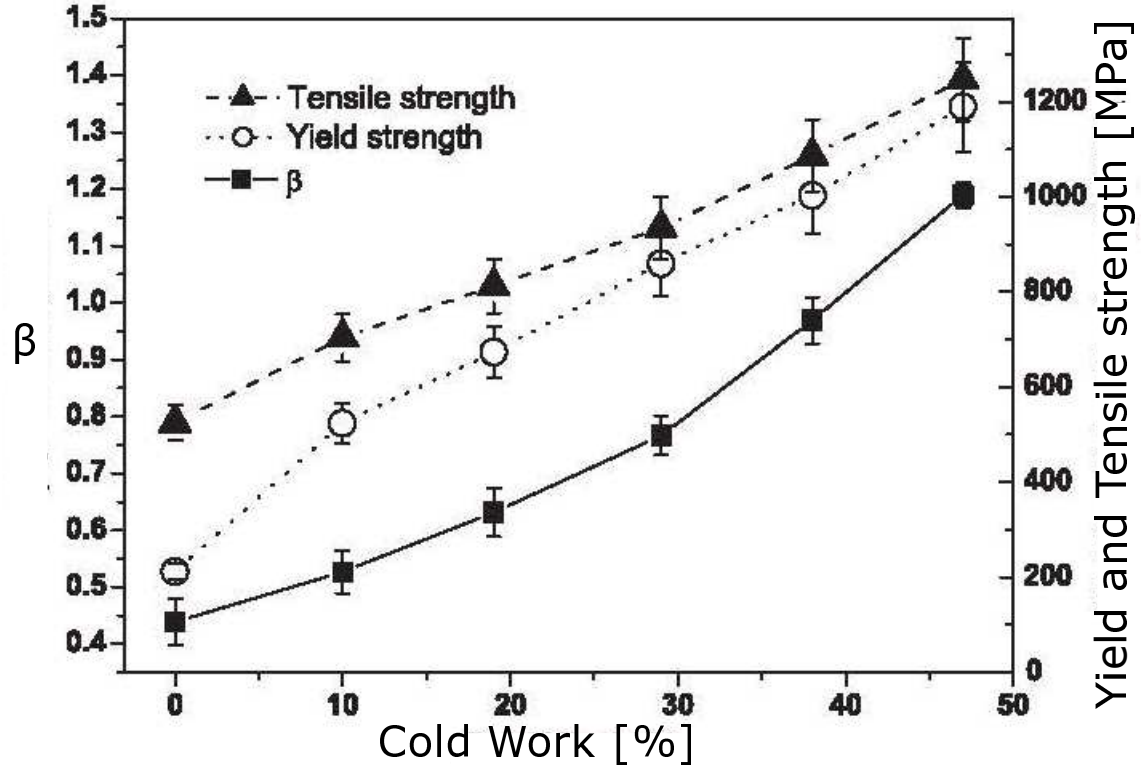

Figure 11: Variation of β, yield strength, tensile strength with increase of cold work in 304 SS [20]

4.3 Effect of cold work and sensitization on 304 ss

Singh et al. discuss their results on the effect of cold working and sensitization on AISI 304 SS in their research paper [17]. They used 304 plates with 8 mm thickness and solution annealed them as a plate, then cut them into various plates. Those plates were unidirectional cold rolled and thickness reduced to 20, 40, 60 and 80 %.

The cold rolled plates were then sensitized for different holding times and temperatures of 600 ° and 700 ° C. The degree of sensitization was measured with the electrochemical potentiokinetic reactivation (EPR) test and displayed in degree of sensitization (DOS).

Figure 12 shows the change of DOS over different holding times and cold rolling. It is obvious that previous cold rolling is enhancing sensitization susceptibility. DOS is not increasing monotonically. In figure 12 a), the degree of sensitization for the 40 % cold rolled specimen is higher than the 60% specimen and the maximum occurs at 1 h.

Another effect that appears is desensitization, which is seen by the rapid decrease of DOS after long holding times. Singh et al. [17] also describes the change in the structure of the steel. During cold rolling, the austenite of the 304 SS transforms to martensite, also known as deformation-induced martensite (DIM), due to the high pressure. The more the specimen thickness is reduced, the more DIM is present.

Singh et al. also show that the grain size changes with cold rolling, but is not affected by the sensitization treatment.

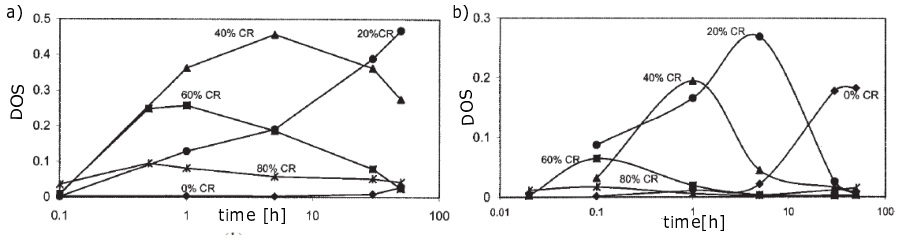

Figure 12: Increase of DOS in cold worked and sensitized 304 SS specimen for a) 600°C and b) 700 °C [17]

CHAPTER V

MATERIAL AND SPECIMEN PREPARATION

5.1 Material

The material investigated on in this research is AISI 304 stainless steel, one of the most commonly used stainless steel in the engineering and power generation industry due to its high variability and corrosion resistance. Unfortunately, different heat treatments and working process can weaken steel and therefore the composition of the material has to be derived more specifically. Table 2 shows the chemical composition in % of 304 SS. Since sensitization is the heat treatment effect focused on in this research, the Chromium amount is the most important composition.

Table 2: Chemical composition of AISI 304 SS in %

Chemical Analysis	C	Mn	P	S	Si	Cr	Ni	Cu	Mo
Nominal composition in %	0.08	2.0	0.04	0.03	1	18	8	0.75	0.75

5.2 Material preparation

The test samples are prepared in different ways, due to the different measurement methods used. Flat bars with a thickness of 0.625 inches, width of 3 inches and a length of 18 inches were solution annealed with a temperature of 1080 ° C for one hour and then water quenched to avoid sensitization effects during the cool down. All of the flat bars were annealed simultaneously to ensure the same baseline for every measurement.

For the longitudinal wave measurement strips with a width of 1.1 inches were cut out, whereas for the Rayleigh wave measurement a width of 3 inches remained. The

reason for the larger width for the Rayleigh wave specimens is caused by the design of the wedge used, which has to be in contact on the surface completly.

The thickness of 0.625 inches fulfills the requirements of at least twice the wavelength for Rayleigh waves at a frequency of 2.5 MHz, so that no reflection from the bottom surface occurs. The 18 inches length of the specimens is long enough to ensure a good cold rolling procedure, but also enough propagation distance for the measurements.

A small phase was manufactured at the beginning of each specimen to lead them more easily into the rolling mills and ensure a better angle during the feed in.

All specimens were surface grinded in the machine shop after the annealing process, then hand polished with GRIT sand paper 2500 and for the EPR tests polished with a brushing wheel. During the surface grinding the specimen are water cooled to avoid potential heat treatment changes and 0.0127 mm are taken off per cut, to induce as less stress as possible.

For the cold rolling the specimens were worked on step by step. Unfortunately, the rolling mill could caused the surface to dramatically change, for example bending, waves and pits. To avoid this condition, the specimens were rolled in small steps, 1-2% steps every time to finally reduce the thickness to the desired amount.

For the sensitization process the specimens were put into the furnace at a temperature of 675 ° C for different holding times, always all together to ensure the same conditions and then air-cooled. The cooling rate was slow enough to avoid internal stresses and therefore not affecting the non-linearity parameter.

After every sensitization step a layer of oxidization settled on the specimen surface, which changes the non-linearity measurements. For that reason every specimen was hand polished after each sensitization step again, providing a clean and flat surface for the measurement procedures.

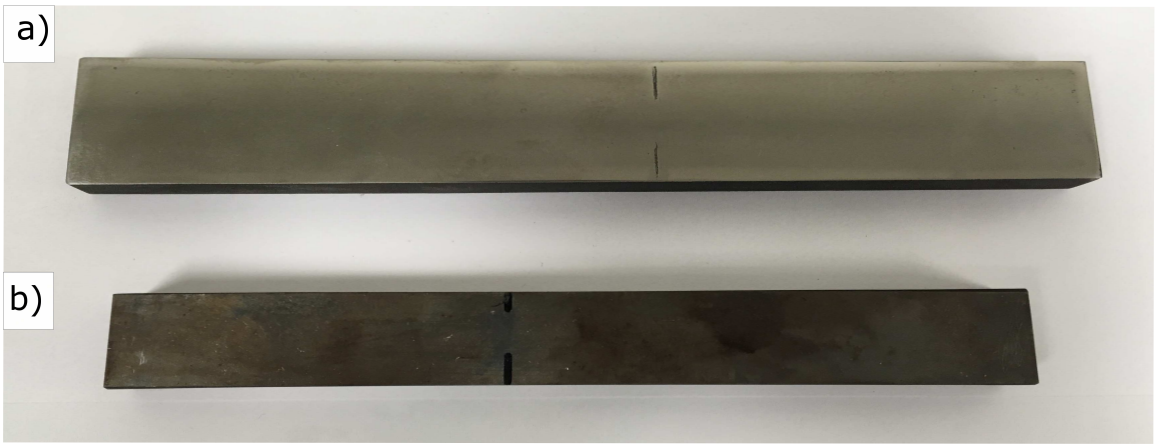

Figure 13: a) a sensitized specimen, hand polished b) sensitized, unpolished specimen

Figure 13 shows the surface differences between a hand polished and an oxidized specimen after the sensitization process. Previous work has shown that the surface structure and condition have great influence on the nonlinearity parameter, β.

CHAPTER VI

MEASUREMENT PROCEDURES

This chapter describes the non-destructive evaluation (NDE) methods used for determining the influence of cold rolling and sensitization on 304 stainless steel. The Rayleigh wave and longitudinal wave methods could be used for field measurements, whereas the EPR is a laboratory based method.

6.1 Rayleigh wave measurement setup and procedure

6.1.1 Function Generator

To induce a signal into the transducer that will travel in the specimen, an AGILENT 33250A 80 MHz function generater is used. It creates a tone burst signal and operates at 2.1 MHz, which enables the best possible signal for the measurement [18] [18].

The peak-to-peak voltage of the sinusoidal signal is 800 mV and has a length of 30 cycles at a burst period of 20ms. The function generator is also necessary for triggering the oscilloscope and RITEC GA-2500A amplifier.

6.1.2 RITEC Amplifier

This sinusoidal signal then gets amplified by a gated amplifier (RITEC GA-2500A), which excites a high voltage signal for the transducer. The high voltage signal is desired so high acoustic energy waves are usable, ensuring the generation of second harmonic waves and a good signal to noise ratio, which leads to more precise results.

The gated amplifier provides the transducer with a stable and clear output signal.

6.1.3 Transducers

6.1.3.1 Oil-coupled transducer

The signal exciting the gated amplifier is then transformed by a 2.25 MHz Panametrics piezoelectric narrow band transducer, to a longitudinal wave. This wave propagates through the plexiglas wedge, hitting the surface of the specimen with angle θ_W, resulting in exciting Rayleigh surface wave in the specimen, which is propagating over a certain distance and leaking waves into the air.

Based on Snell's law the angle of the wedge, θ_W, seen in figure 14 can be determined by using wave speed, c_P in the plexiglas wedge and wave speed in the specimen, c_R, which is a Rayleigh wave.

$$\theta_W = arcsin \frac{c_P^{wedge}}{c_R^{specimen}} \tag{61}$$

To ensure good coupling conditions and decrease the loss of wave energy approximately, the same amount of oil between transducer-wedge and wedge-surface is used. The oil is set for 30 minutes so it can distributed equally over the contact surface and the conditions for every measurement is nearly the same for every measurement. By grinding and polishing the specimen surface before the measurements, the surface conditions are at its optimum and Aceton is used to remove dirt.

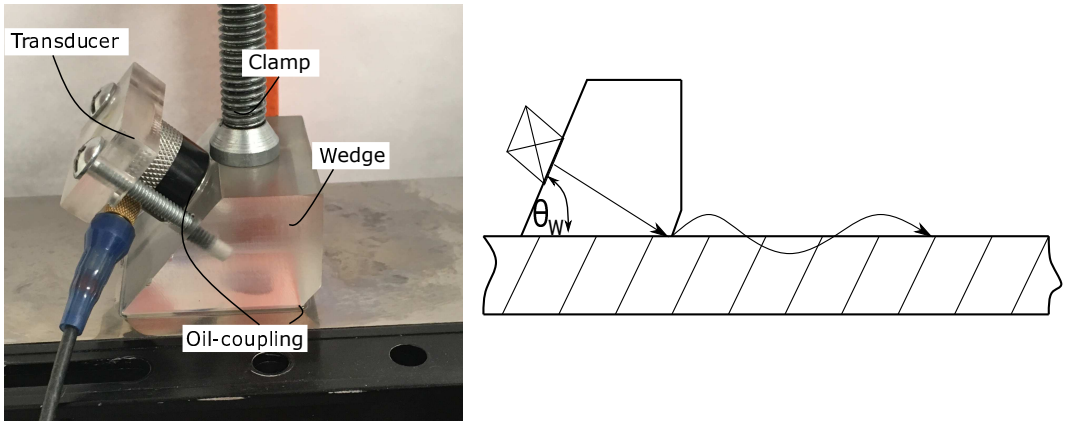

Figure 14: Setup of wedge on the specimen surface and wedge ankle, θ_W

The transducer is held with two screws onto the wedge, while the wedge is clamped

down onto the surface with the approximately the same clamping force after every setup. Unfortunately, the contact conditions between wedge and surface can not be made perfectly equal every time, inevitably leading to small variations in the resulting β. Figure 14 shows how the wedge is hold on the specimens surface, the oil coupled sections and the wedge ankle, θ_W.

6.1.3.2 Air-coupled transducer

As already mentioned the Rayleigh waves propagating over the surface of the specimen are leaking longitudinal waves in the air, which can be detected by an air-coupled transducer (Ultran NCT4-D13), which was implemented and tested by Thiele [18].

This transducer has a bandwidth of up to 4 MHz and the fixture device has 4 degrees freedom in motion. This is necessary to capture the highest signal leaking of the surface.

6.1.4 Post Amplifier

The output signal of the air-coupled transducer has a very small, not displayable for the oscilloscope, 1mVpp Voltage. A Parametrics 5676 PR pulse receiver is post amplifying the signal, obtaining a sufficiently high signal-to-noise ratio. The amplifier works at 40dB.

6.1.5 Oscilloscope

This signal is then captured by the oscilloscope, which averages the 512 waveforms over a one time-domain signal. This signal is post-processed for the data analysis, leading to the nonlinearity parameter,β. The sampling rate is at 500Ms/s.

A schematic of the setup of the Rayleigh wave measurement procedure is shown in figure 15.

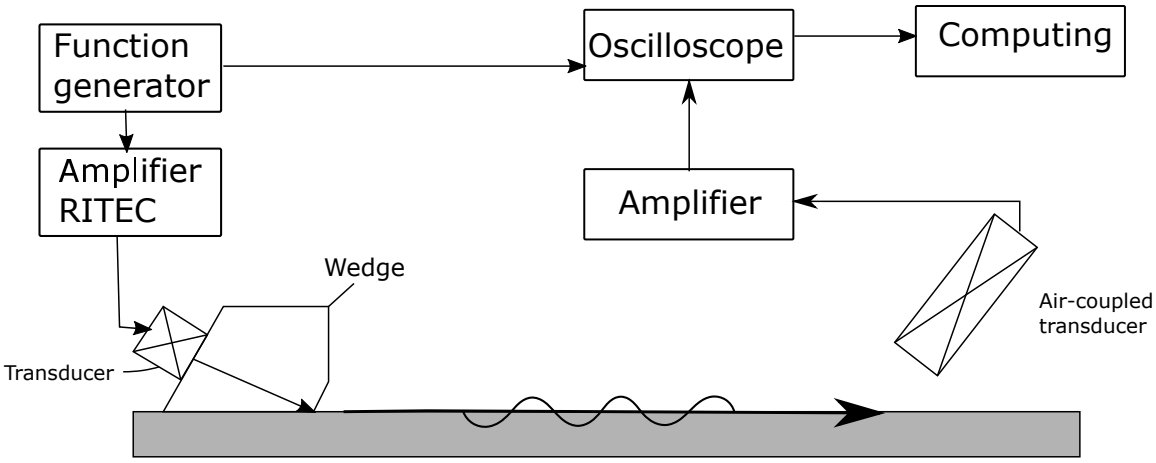

Figure 15: Rayleigh wave measurement setup

6.1.6 Measurement procedure

After setting up the function generator and gated amplifier (RITEC), preparing the transducer and wedge and coupling them with oil lubricant, the actual measurement can be performed. As already mentioned, it is important to let the lubricant settle for 30 minutes, so it gets distributed equally, as well as the Amplifiers after turning them on.

The coupling between wedge and specimen has to be changed after every measurement, whereas the coupling between transducer and wedge can be used for several days. This eliminates one possibility of measurement fluctuations, since this condition is held constant.

Thiele [18] describes in his work that due to the material, machines and system, the wave does not propagate on a perpendicular path from the wedge. The leaked longitudinal waves spread over a wide area and can be captured by the air coupled transducer, but it is necessary to catch the highest signal over propagation distance, which can be seen in figure 16. The Rayleigh wave is not propagating on a path perpendicular to the wedge front, it is deflected and in order to capture the highest signals, the air coupled transducer is moved after the calibration on the deflected

path. In this work the steps were 1.5 mm, or 2.5 mm for each measurement point. To capture the peak of the signal a calibration process is used, where the angle of the air-coupled transducer and the x_2 position at the $x_{1,min}$ and $x_{1,max}$ is determined.

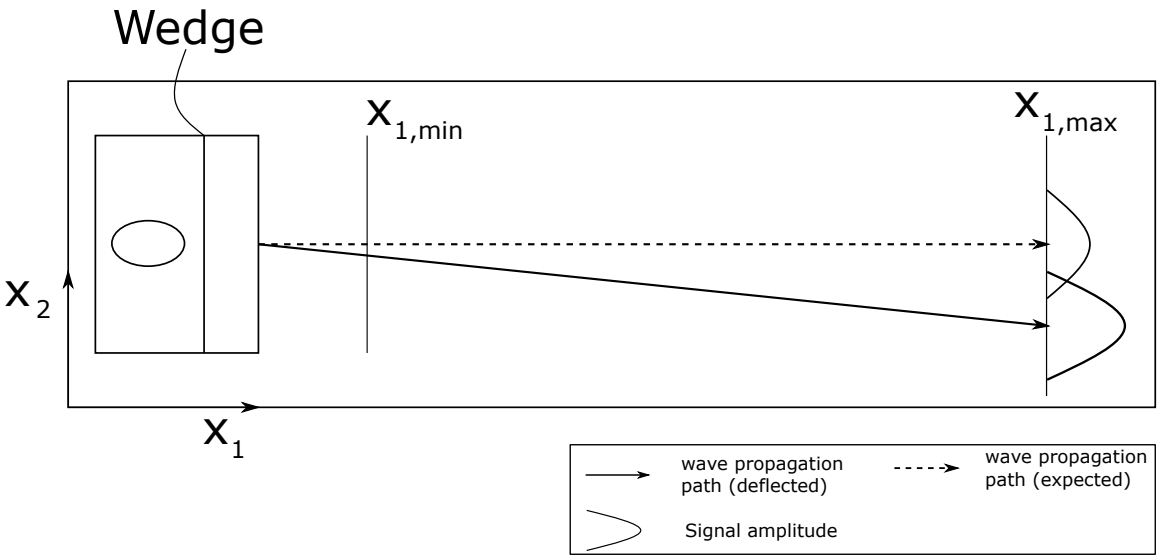

Figure 16: Propagation path of Rayleigh wave on the specimen surface (top view)

For the calibration, measurement sets are taken at different angles at the same spot and also measurement sets for different x_2 values at $x_{1,min}$ and $x_{1,max}$. Thiele [18] showed that ideal assumptions can be made and that for the x_2 calibration the peak of the linear fit can be used, whereas the angle, which also could be calculated with Snell's law, which would be too inaccurate, has to be determined precisely by the highest measurement point, since it has a higher influence on the signal amplitude.

Figure 17 displays the results of the angle calibration at $x_{1,min}$. For that measurement an angle of 5.9 ° was used. Since the fundamental wave A_1 has a higher amplitude than the second harmonic, the calibration is based on the fundamental. Additionally, the x_2 position with the highest signal at $x_{1,min}$ and $x_{1,max}$ are detected and the assumption is made that the wave propagates linearly between those.

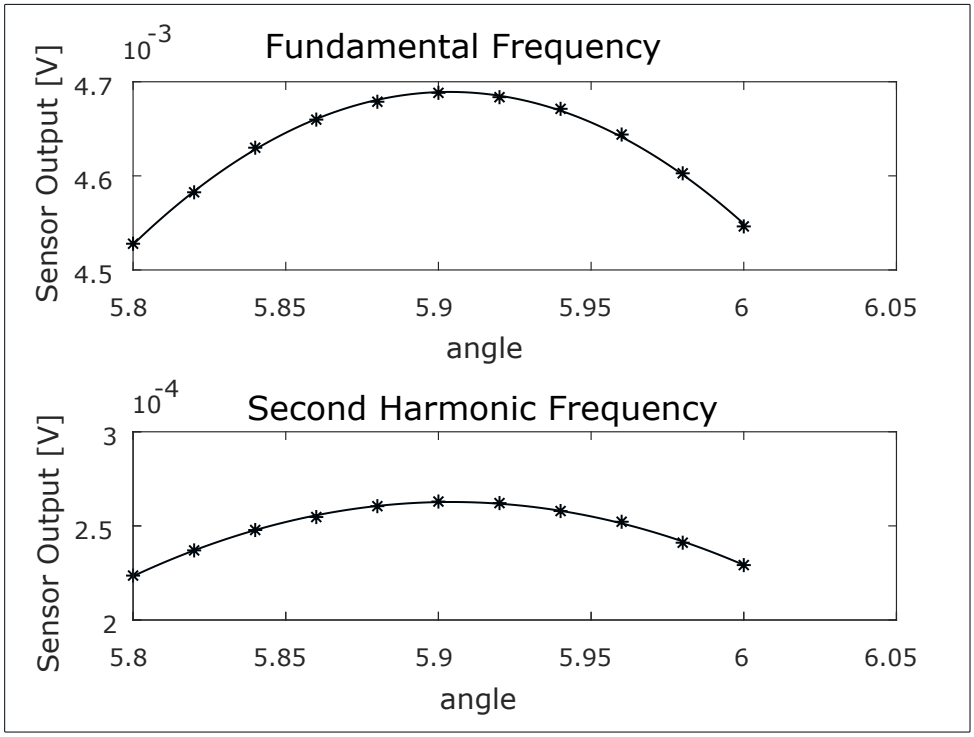

Figure 17: Angle calibration at $x_{1,min}$ for the Rayleigh wave measurement

After the calibration the actual measurement process takes place, where the air coupled transducer is moved over the surface of the specimen. The lift off distance between the air-coupled and the surface is 2 mm and starting point $x_{1,min}$ is 2 mm from wedge to edge of the air-coupled, when its bent at 6 °. A measurement point is taken every 2.5 or 1.5 mm, depending on the total propagation distance aimed for. The air-coupled transducer is following a linear path from $x_{1,min}$ to $x_{1,max}$ and during every measurement step the x_2 axis is adjusted

The propagation distance measured in this work is either 50 mm or 30 mm from the wedge. Due to the cold rolling the specimen surface became undulatory, which affects the Rayleigh wave measurement enormously. Therefore, smaller propagation distances had to be chosen, where no significant waviness occur on the surface. Another reason is the attenuation effect appearing for the second and fundamental harmonic. The effect of attenuation and distribution and the surface waviness lead to

the optimum propagation distance of 30 mm.

With this result the nonlinearity parameter, β is calculated, but further described in chapter 6.1.7.

6.1.7 Data Analysis

All the devices used as the amplifier, function generator and transducers, contribute to the nonlinearity in the material. Because of the changing coupling conditions and clamping forces during each measurement it is not possible, to calculate an absolute value of the nonlinearity parameter, β, and therefore the relative nonlinearity parameter, β', was introduced in 3.5.1. Doerr [6] and Thiele [18] proved that the relative nonlinearity parameter is still useful to compare and investigate the effects of stress and heat treatment in 304 specimens.

To determine β', the exciting signal of the air-coupled transducer is averaged by the oscilloscope. It is a time domain signal of the fundamental and second harmonic and has to be transformed into a frequency domain signal in order to be expressive.

Figure 18 a) is displaying the averaged time domain signal of the Rayleigh wave measurement. A Hanning- filter window is used to neglect ringing effects and unnecessary noises and a peak detection code is used for using the middle 15 peaks of the signal, since transducers and machines are influencing the outermost peaks to drastically. With a Fast-Fourier Transform (FFT) the time domain signal is transformed into a frequency-domain signal, seen in figure 18 b).

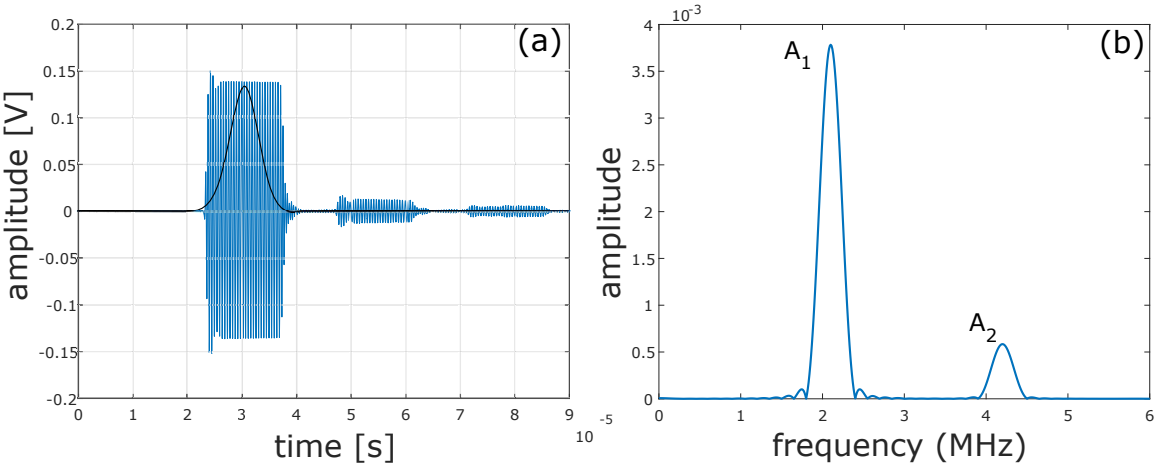

Figure 18: a) Averaged time-domain signal of air-coupled transducer b) Frequency domain signal after FFT

With the frequency domain signal the fundamental, A_1, and second harmonic waves, A_2 can be displayed over the propagation distance. Due to attenuation affects and spreading of the waves, A_1 is decreasing over propagation distance, while A_2 is increasing in the beginning, but after a certain distance attenuation effects are taking over, resulting in a decreasing A_2 amplitude. The progression of A_1 and A_2 are pictured in figure 19.

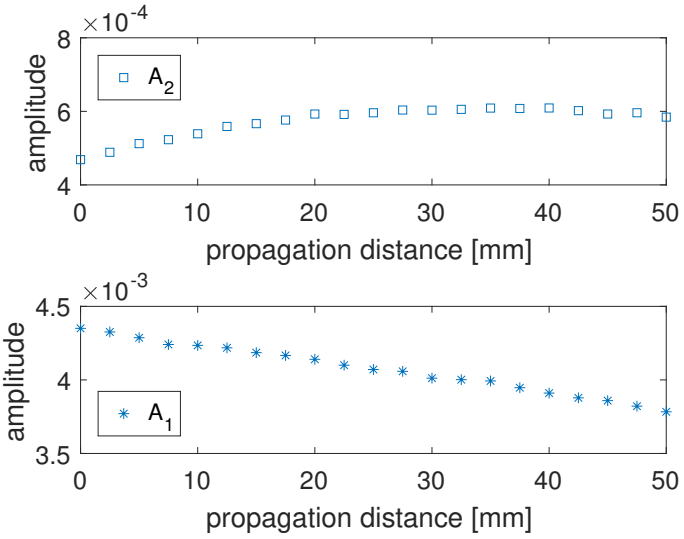

Figure 19: Fundamental and second harmonic waves over propagation distance

Using equation (60) and the amplitudes plotted in figure 19 the relative nonlinearity parameter, β', can be calculated. The measurement points are nearly increasing linearly, nonetheless a linear fit is put over them. The slope of the linear fit equals β' and gives information about the nonlinearity changes in the material and can be seen in figure 20.

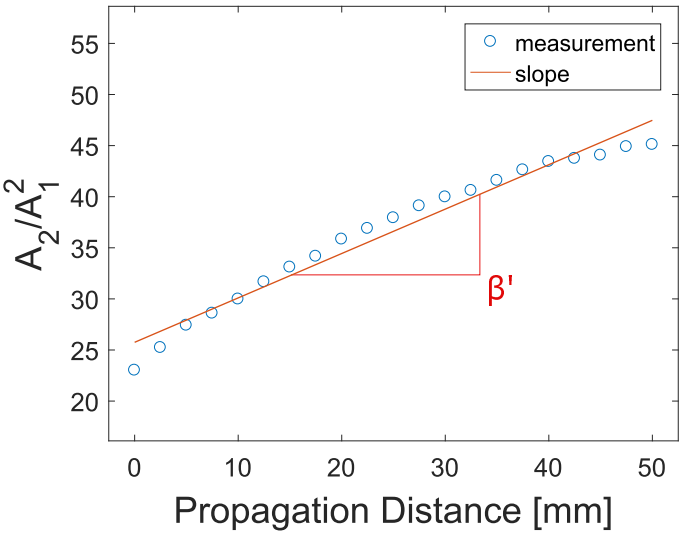

Figure 20: Fundamental and second harmonic waves over propagation distance

6.2 Longitudinal wave setup

6.2.1 Measurement Setup

For the longitudinal wave measurement the specimens are clamped between two piezoelectric transducers. The 5 MHz transducer is indicating longitudinal waves through the material and a 10 MHz transducer is capturing the first and second harmonic waves on the opposite side of the material. To ensure good contact conditions a specially designed device is used to align the two transducers perfectly and to make sure that the positions are nearly the same for every measurement. Three or four measurements were taken on each specimen at the exact same point and the transducers were taken off and clamped again every time. A light oil coupling was used between transducers and material to ensure efficient transmission of the waves.

The setup and machines used are very similar to the Rayleigh wave setup described in chapter 6.1. The function generator induces a sinusoidal signal of 5 MHz and 19 cycles, which is increased by the RITEC amplifier and transmitted to the transducers. This signal is captured and 512 times averaged by the oscilloscope and then transferred to a computer for processing and data analysis.

Figure 21 shows the systematic setup and signal flow of the longitudinal measurements. Unlike the Rayleigh wave measurements, where the Power Level of the amplifier is hold constant for every measurement and the propagation distance is changed, the RITEC amplifier Power Level is increased during the measurement from 6.2 to 7.2 V in 0.04 V steps. As a result of that A_1 and A_2 increase and β' can be calculated.

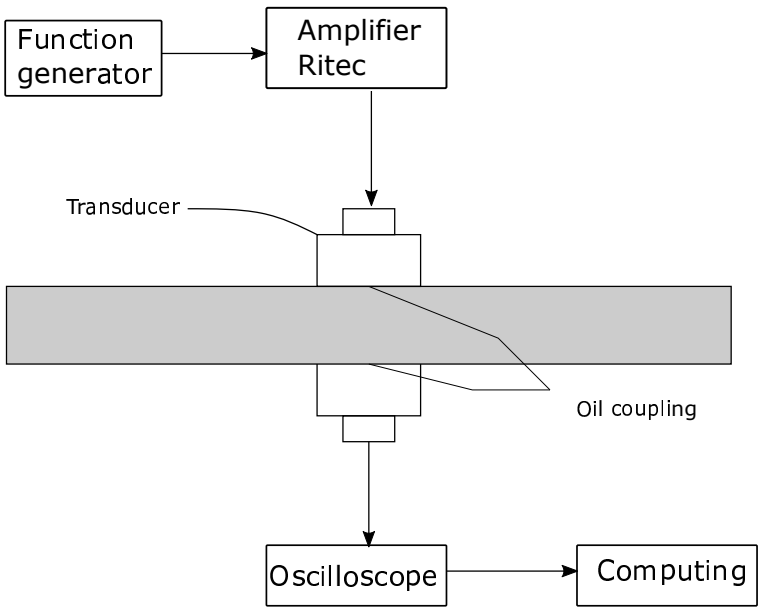

Figure 21: Longitudinal wave measurement setup

6.2.2 Data-Analysis for Longitudinal wave measurement

Similar to the data-analysis for the Rayleigh wave measurement described in chapter 6.1.7, the time domain signal captured and averaged by the oscilloscope is used to determine the nonlinearity parameter, β'. A Hanning window and a FFT is put over the time domain signal, resulting in a frequency domain signal of the first and second harmonic waves. With the frequency domain signal and equation (60) a curve for A_2 over A_1^2 is calculated. A linear fit is put over the measurement points and the slope of this fit is resembling the parameter β'.

Figures 22, 23, 24 and 25 show the first and second harmonic in the time- and frequency domain signal and the linear curve fitting resulting in β'.

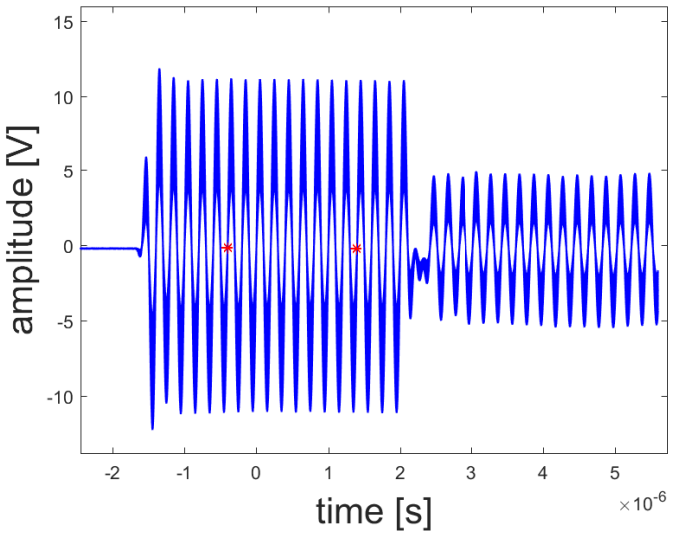

Figure 22: Averaged time-domainsignal for longitudinal measurement

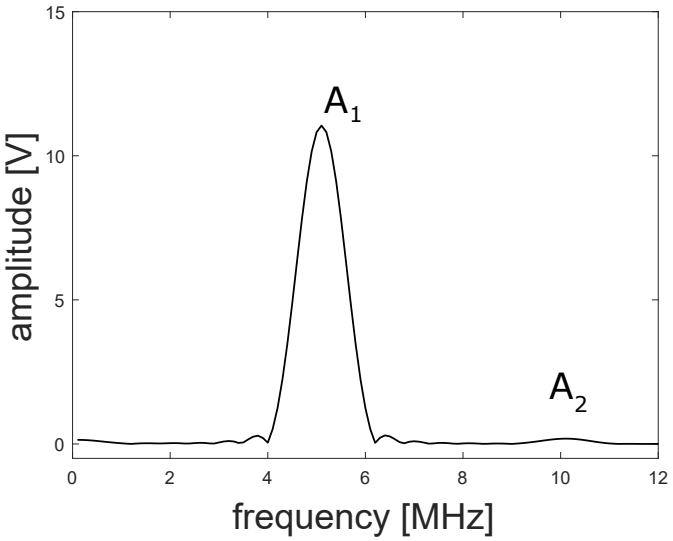

Figure 23: Frequency domain signal after FFT and Hanning window

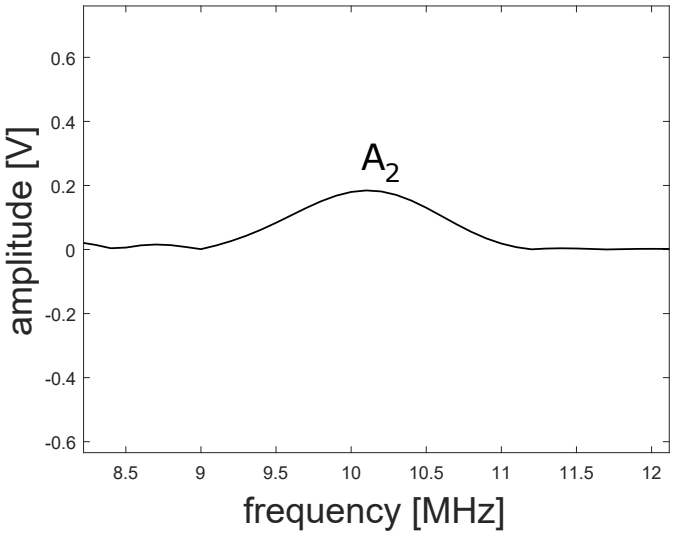

Figure 24: Maximized view of figure 23 on second harmonic

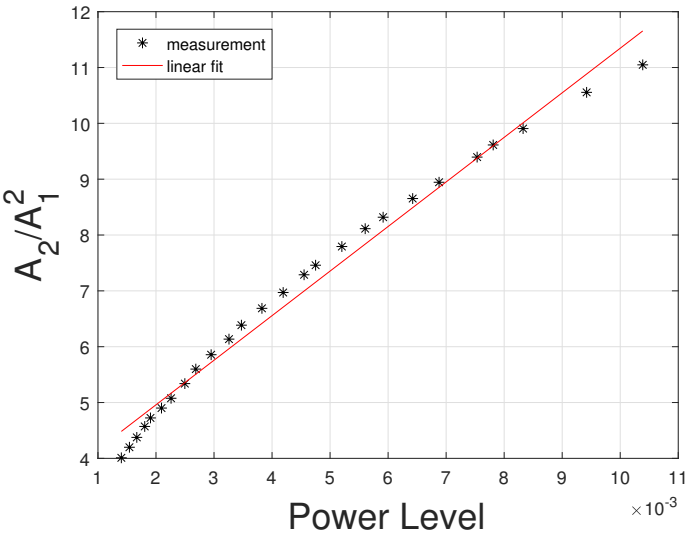

Figure 25: β' over change of Power level for longitudinal measurement

6.3 Electrochemical potentiodynamic reactivation process (EPR)

To ensure and support that sensitization actually is taking place in the 304 SS specimens, the electrochemical potentiodynamic reactivation (EPR) ASTM G108 measurement method was used. This method provides a nondestructive means and quantifies

the degree of sensitization (DOS) of 304 SS. It is a widely accepted method and also can be used for different materials as Nickel or other stainless steels. DOS gives exact information if sensitization and therefore chromium depletion at the grain boundaries occurred.

To accomplish the test a potentiodynamic sweep from the passive to the active regions takes place. The amount of charge in correlation with the chromium-depleted regions is measured. These carbide precipitates are susceptible to corrosion in oxidizing acid solids, causing a rise in the current density.

The EPR test is reproducible as long as temperature, composition and scan rate are carefully controlled and hold as constant as possible. Figure 26 displays the difference in DOS of a sensitized and non-sensitized 304 specimen. It is obvious that the peak for a sensitized material is larger than it is for a non-sensitized. Sensitized steels are easily activated and therefore show a higher current density. The value of DOS is normalized to a not-sensitized specimen.

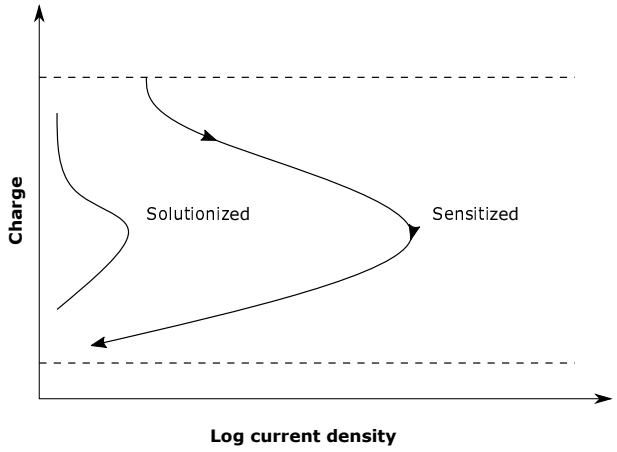

Figure 26: EPR test results [2]

6.3.1 Measurement setup and procedure

The EPR apparatus consists of electronic instruments and a test cell, often integrated into one instrument package. The typical setup for an EPR measurement is illustrated

in figure 27 and uses a scanning potentiostat, potential measurement instrument, a current integrated measuring instrument, holding aperatus for the specimen and a test cell [2].

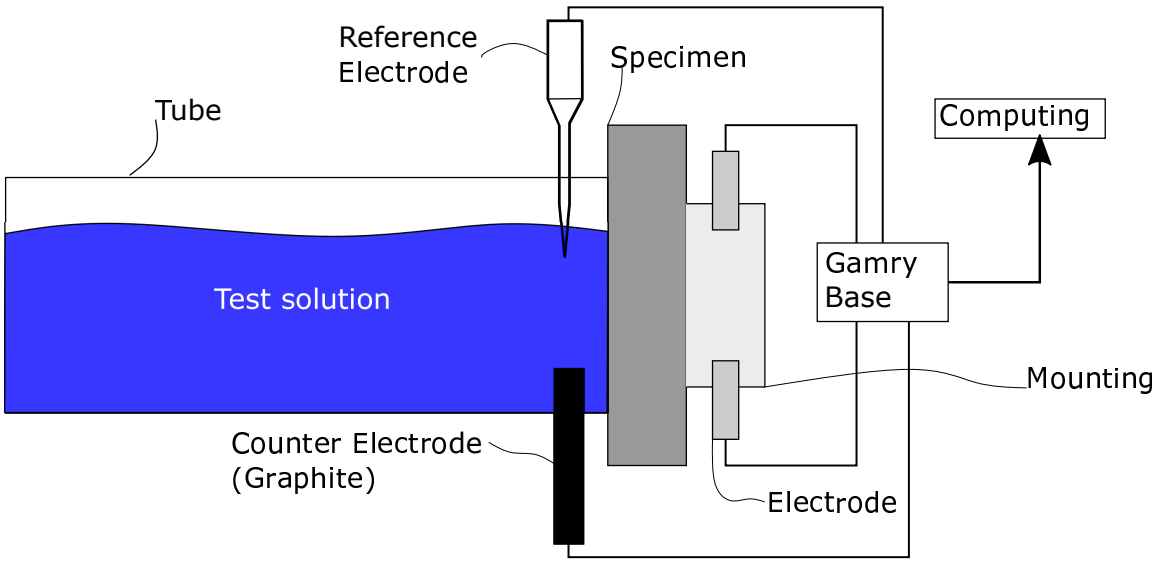

Figure 27: EPR setup for investigation on sensitized 304 specimen

After the specimens are heat treated in the furnace, the surface has to be polished to remove the oxidation layer, which would have a huge effect on the DOS. Therefore, the surface is hand grinded with up to 600-grit paper and finished with 6 and 1 μm diamond paste on a polishing wheel.

Before the measurement, the test solution has to be prepared. It consist of a mixture of reagent sulfuric acid (H_2SO_4) and potassium thiocyanatae (KSCN), solved as 0.5 M of H_2SO_4 with 0.01 M KSCN in one liter of distilled water. The mixture can be stored for one month at room temperature and is still usable.

For one test approximately 500 ml of solution is needed in the solution cell. First the open circuit potential (OCP) is recorded for up to 2 min. After that the reactivation scan takes place, starting with a the rate of 1.67 mV/s, causing a decay in the current density. For capturing the data and changes in DOS a Gamry 600 base and analysis tool was used, which is measuring and showing the peak of the DOS.

These peaks, as seen in figure 26 give information about the sensitization amount in the specimens and makes it comparable to the nonlinearity parameter of the Rayleigh and longitudinal wave measurements.

Figure 27 shows the scanning and reference potentiostat electrode, as well as the solution cell and the specimen holding apparatus. The graphite electrode is used as a counter electrode and a reference.

CHAPTER VII

RESULTS AND DISCUSSION

7.1 Results of Rayleigh wave measurement on cold rolled specimen

In this section the results for the Rayleigh wave measurement on cold rolled specimen are shown. Due to the problem of undulation after cold rolling on the specimen surface and adjusting to that effect, the Rayleigh wave measurement was only made on cold rolled specimen and a not rolled, but sensitized specimen.

7.1.1 Rayleigh wave measurement on cold rolled 304 SS

The propagation distance measured for the Rayleigh wave measurement was adjusted and differs from that in the work of Doerr [6] and Thiele[18], who used a propagation distance of 50 mm. In this work a propagation distance of 30 mm was chosen to neglect the effect of dispersion and attenuation, which increases after a propagation distance of 35 mm, which results in a decrease of the second harmonic A_2.

A series of ultrasonic measurements on cold rolled specimen were made, where each measurement was taken after every cold rolling step. The specimen was annealed as well, then surface grinded and measured. After that it was cold rolled and measured after every thickness reduction.

Figure 28 shows the effects of cold rolling on β. With increase of cold work in the material, the nonlinearity β of the Rayleigh wave increases. The small decrease from 0-6% cold rolling is expected to be a measurement error. Another reason could be the too small deformation that the grains are undergoing and therefore β is not sensitive to a small amount of cold roll. After a cold rolling amount of 11%, an obvious increase of β is visable that is 21%. This shows that due to cold work, the grains deform and

Table 3: Results for cold rolled specimen, without surface grinding after cold rolling

cold work [%]	0	6	11	20
β	1	0.98	1.21	1.31
standard deviation [%]	8	7	5	8

get an ellipsoidal shape. This change of grain size and shape is detectable by Rayleigh (shear waves). The data of the averaged cold rolled β is shown in table 3.

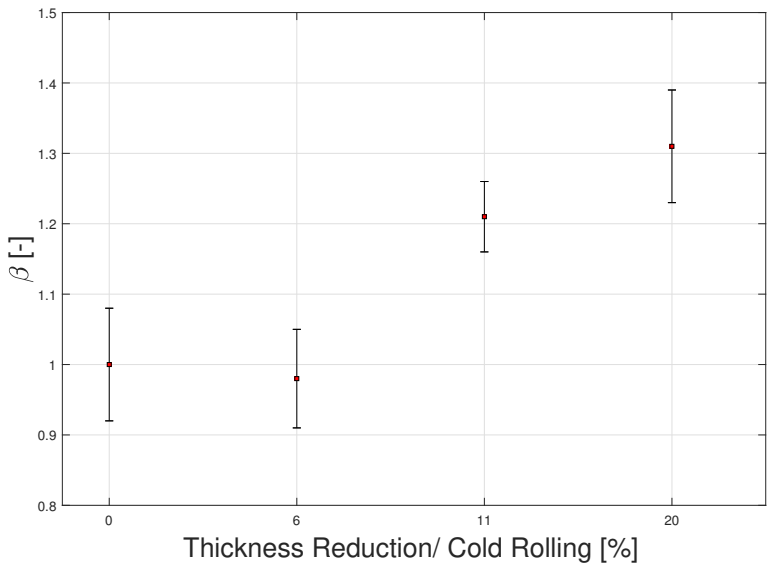

Figure 28: Results for Rayleigh wave measurement on cold rolled specimen, without surface grinding after rolling

7.1.2 Failed Rayleigh measurements

Figure 29 shows the results of the first measurement on the cold rolled specimen for a propagation distance of 30 mm. For this measurement setup 6 different specimen were prepared, annealed together in the furnace, surface grinded, then cold rolled (each specimen to a specific amount) and surface grinded again to get a flat surface for the measurement. β then was normalized to an annealed, but unrolled specimen. As figure 29 displays, β follows an unpredictable path, increasing up to 13%, followed by a tremendous drop and increase again. The relatively large error bars are due

to many measurment points on the surface, where the coupling condition (clamping force and amount of oil) changed after every measurement. It is nearly impossible to hold these factors constant, since it is done by hand.

Furthermore the assumption was made that by surface grinding the wavy surface after cold rolling, the compressed layer is removed. Cold rolling is still traceable, for example with magnetic measurements showed by Mumtaz et.al [12], but a huge amount of cold worked layer was taken off during the grinding process. Table 4 shows the data used for figure 29 and the calculated, normalized error bars.

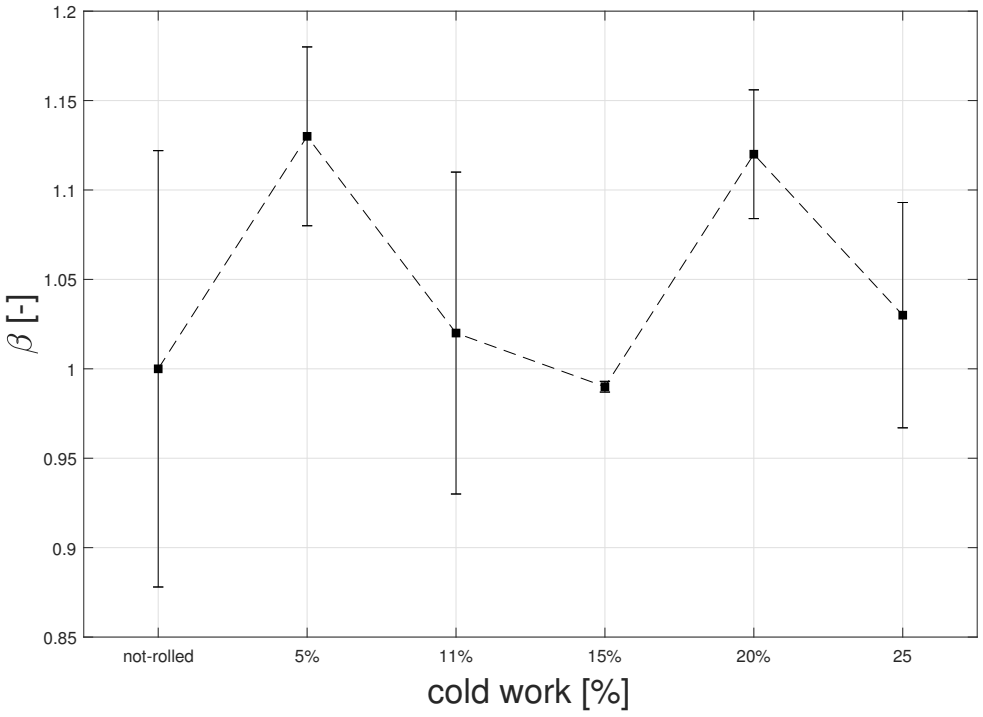

Figure 29: Results for Rayleigh wave measurement on cold rolled, then surface grinded specimen

Table 4: Results for cold rolled specimen, surface grinded after cold rolling

cold work [%]	0	5	11	15	20	25
β	1	1.13	1.023	0.99	1.12	1.03
standard deviation [%]	12	4.6	8.5	0.3	3.6	6.3

7.2 Results of longitudinal wave measurements on cold rolled and sensitized specimen

As a comparison to the Rayleigh wave measurements on cold rolled 304 stainless steel, longitudinal wave measurements were made. Three different specimens were used, annealed and water quenched together to have the same 'baseline' and then cold rolled to 7 and 16%. After the cold rolling and annealing the surface was hand polished with sand paper GRIT 2500 to remove the oxidation layer and to provide equal surface conditions.

Figure 30 shows the result of the longitudinal measurement on these specimens. The results are averaged and normalized to the unrolled (0% cold work) specimen. As it can be seen, β increases significantly from 0% to 16% by up to 24% in total, whereas the step between 0% cold work to 7% cold work is smaller (9% increase). The increase of β is due to the plastic deformation the grains are experiencing during the cold rolling. As already mentioned before it is assumed that rolling changes the shape of the grains from spherical to ellipsoidal grains and additionally martensite is induced due to the pressure. The more the thickness is reduced, the 'flatter' the grains will get, resulting in dislocations of grains and crystall gratings. Table 5 shows the data used for figure 30.

Table 5: Results for the longitudinal wave measurement on cold rolled 304 specimen

cold work [%]	0	7	16
β	1	1.09	1.24
standard deviation [%]	3.7	2.7	1.3

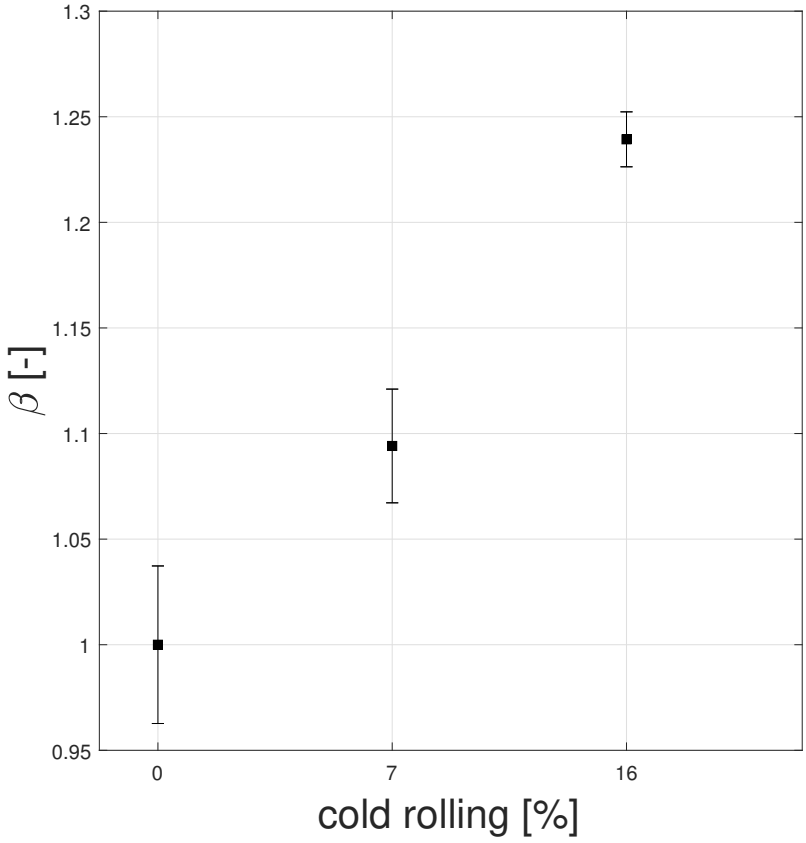

Figure 30: Results for longitudinal wave measurement on cold rolled specimen

These three cold rolled specimens were then used for the sensitization process. They were put into the furnace together at a temperature of 675 °C for different holding times, then air cooled. After every sensitization step the surface was hand polished with sand paper GRIT 2500.

Figure 31 displays the results for 0,7 and 16 % cold rolled specimen for holding times up to 3 h. For each sensitization step three or four measurements were taken and the resulting β is averaged and normalized to each β value at a holding time of 0 minute. The data used for figure 31 can be seen in table 6, as well as the standard deviation for each specimen. The changes of β for all three specimen are minor and in a range of $\pm$ 10 %. This leads to two conclusions: Either, longitudinal

wave measurements are not sensitive to the thermal changes induced by sensitization, therefore not sensitive to chromium precipitation, or the effect of cold rolling, thus the effect of dislocated grains and grain deformation is the prevailing effect measured. For the unrolled specimen a small increase in β over holding time is visible, supporting this assumption. This would lead to the definition of β as:

$$\beta_{all} = \beta_{coldroll} + \beta_{sensitization} \tag{62}$$

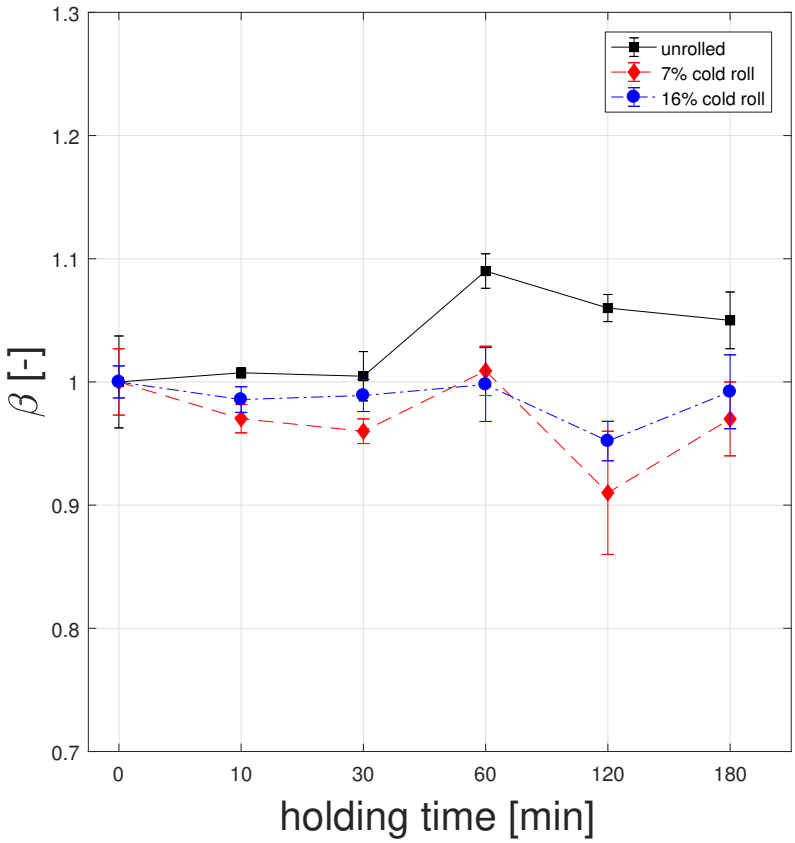

Figure 31: Results for longitudinal wave measurement on cold rolled and sensitized 304 specimen

Table 6: β results for cold rolled and sensitized 304 specimen

cold work [%]	holding time [min]	0	10	30	60	120	180
0	β	1	1.007	1.004	1.09	1.06	1.05
	standard dev. [%]	3.7	0.4	2	1.4	1.1	2.3
7	β [-]	1	0.97	0.96	1.009	0.91	0.97
	standard dev. [%]	2.7	1.1	1	2	5	3
16	β [-]	1	0.99	0.99	0.998	0.95	0.99
	standard dev. [%]	1.3	1.04	1.3	3	1.6	3

7.3 Comparison of longitudinal wave results with previous work

As already mentioned in chapter 4.2, Viswanath et al. [20] made longitudinal wave measurements on cold rolled 304 SS. Figure 32 displays the results and makes them comparable to the results of this research. Both β values are normalized to an unprepared (not rolled) 304 specimen. Unfortunatly, not the same cold rolling steps were taken for both measurements, but the β values appear in the same range. For example, the results for this research for a 7% thickness reduction lead to an 9% increase of β, whereas Viswanath shows that a 10% reduction increases β up to 15%. It can be assumed that the longitudinal wave measurements made on the 304 SS are correct.

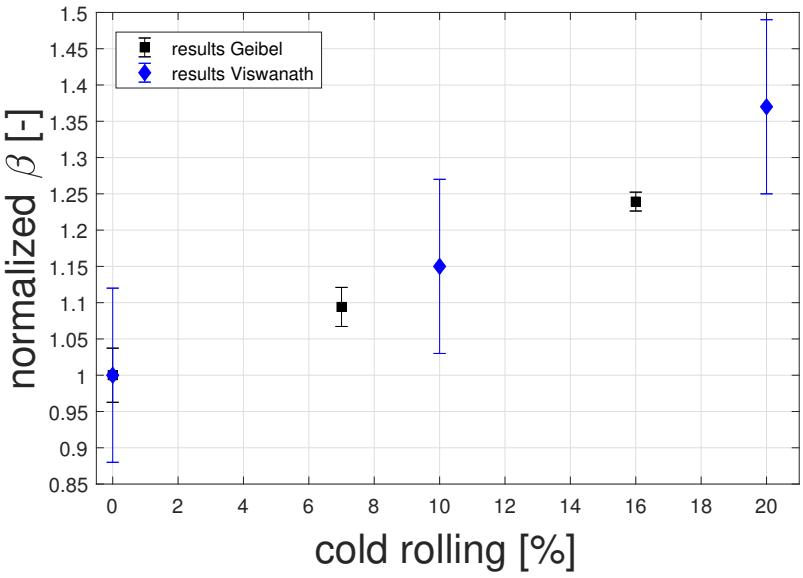

Figure 32: Comparison of Viswanath et al. [20] and results for longitudinal wave measurements on 304 SS made in this research

7.4 Comparison of Rayleigh wave and Longitudinal wave measurements

7.4.1 Comparison of β on cold rolled 304 SS

Comparing the results for the Rayleigh wave and longitudinal wave measurement on cold rolled stainless steel shows that both measurements are sensitive to grain deformation and dislocation due to cold rolling. Putting figure 28 and figure 30 together leads to figure 33. For the two ultrasonic measurement methods differently prepared specimen were used and they are not cold rolled to the same amount. Every β value for each measurement method is normalized to the unprepared (unrolled) β result. Nonetheless it is possible to compare them to each other. The value of β for the longitudinal wave measurement is at 24%, whereas the β for the Rayleigh measurement at 12% cold rolling is at 22%. Measurement uncertainties and therefore the error bars have to be taken into consideration, supporting the approximately same β value for both measurement methods. Unfortunately this theory is not true

for smaller thickness reductions, as it can be seen for 6%, where the β value for the Rayleigh measurement drops. As mentioned before, it is assumed that this drop was a measurement error.

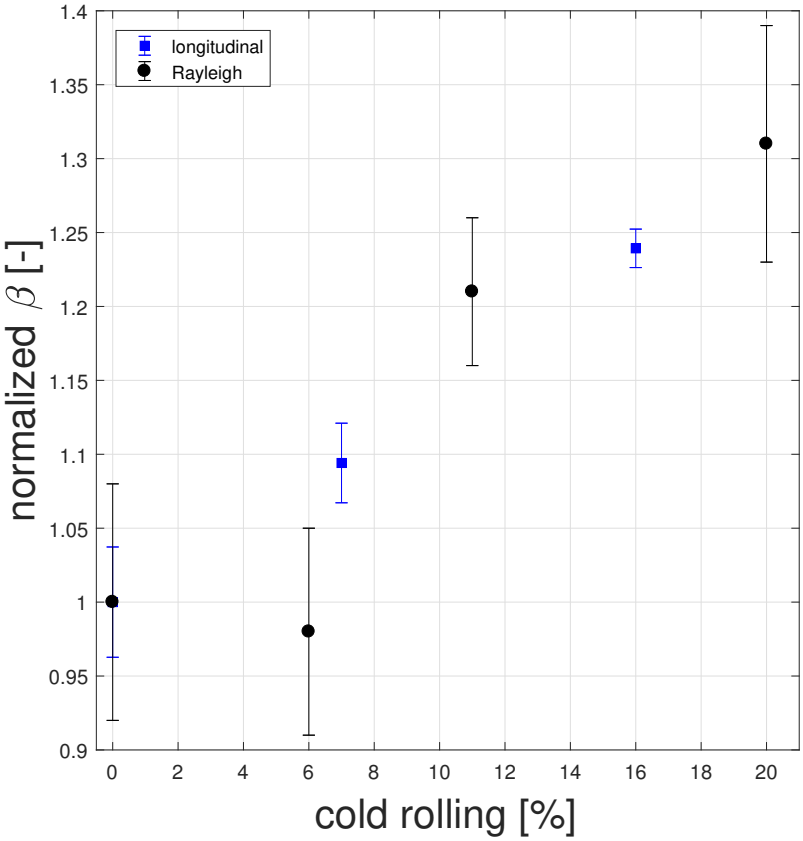

Figure 33: Comparison of Rayleigh wave and Longitudinal wave measurement on cold rolled 304 stainless steel

7.4.2 Comparison of β on sensitized 304 SS

As seen in figure 31, it seems that longitudinal waves are not sensitive to precipitation of chromium during the sensitization process, whereas Doerr [6] showed that Rayleigh waves are sensitive to sensitization. To support that theory, another measurement set was made on two 304 specimens that were annealed and water quenched together, then surface grinded with sand paper GRIT 2500 after annealing and sensitization. One

of the specimen was measured with Rayleigh waves, the other one with longitudinal waves. The holding time of 240 minutes was chosen out of the results of Doerr. He found out that the largest increase of β is happening at that temperature and therefore we can ensure that sensitization took place in the material. The results of those measurements are shown in figure 34 and the values are normalized to β measured for the unprepared specimens. While β of the Rayleigh wave measurement is increasing 26% after a holding time of 240 minutes, β for the longitudinal measurement does not increase. The 26% increase for the Rayleigh measurement is also comparable to the results Doerr [6] had for his measurements. The data used for figure 34 is seen in table 7.

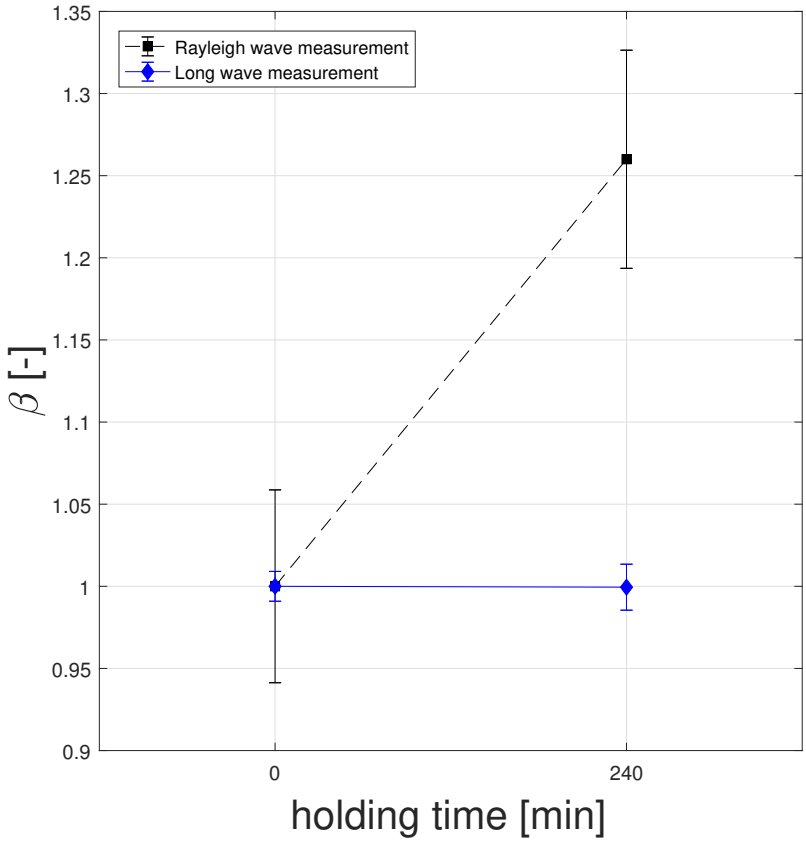

Figure 34: Comparison of Rayleigh wave and Longitudinal wave measurement on sensitized 304 stainless steel

Table 7: Results for Rayleigh wave and longitudinal wave measurement on sensitized 304 stainless steel

	Rayleigh		Longitudinal	
holding time [min]	0	240	0	240
β [-]	1	1.26	1	0.99
standard dev. [%]	5.9	6.6	0.9	1.4

7.5 EPR results on cold rolled and sensitized specimen

Additionally to the longitudinal wave measurement, an EPR test was made on the same specimen used for the results illustrated in figure 31. Between every sensitization step, first the longitudinal wave measurement was made, followed by the EPR test. The results were normalized for each specimen to the holding time of 0 minute. The surface of the specimen were polished with a polishing wheel and diamond paste to ensure perfect condition for testing. The objective of EPR tests was to see, if sensitization is taking place in the specimen at all and what influence the cold rolling has on the DOS. Therefore three specimens, not cold-rolled, 7% and 16% cold rolled, were used and sensitized simultaneously in the furnace for different holding times. The results are illustrated in figure 35. DOS is an absolute value measured, normalized to a holding time of 0 minutes. It can be seen that the degree of sensitization increases for all three specimen over holding time, but stabilizes after 120 minutes. At that point the material is sensitized to its maximum and no chromium can precipitate anymore. Nonetheless, the 16% cold rolled specimen is experiencing more sensitization, resulting in a higher DOS value. This could be the result of the dislocating grains due to cold rolling, leaving small holes in between, making precipitation easier. A tremendous difference in DOS occurs between 16% and the 7% cold rolled specimens. At a holding time of 120 minutes, the 16% cold worked reaches a value of 210, whereas the 7% has a DOS of 40. Table 8 shows the numerical results for the EPR test seen in figure 35 on sensitized and cold rolled specimens.

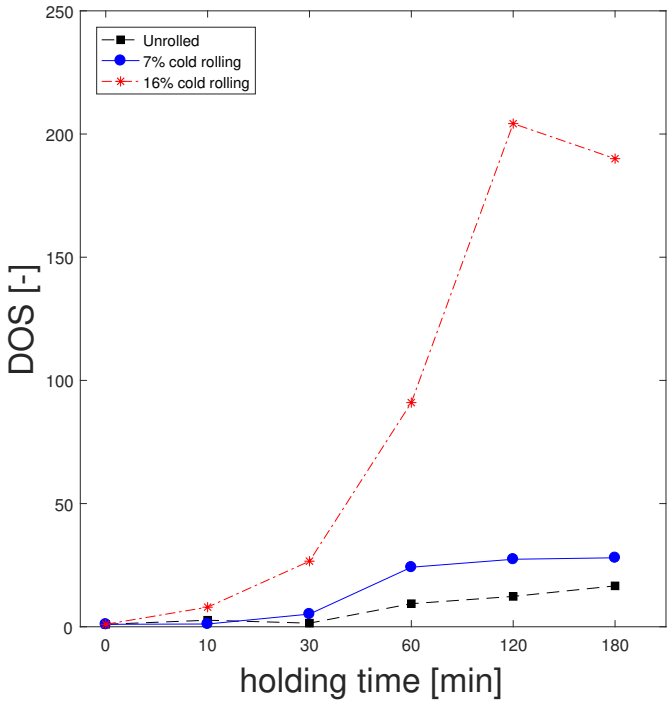

Figure 35: Results for the EPR measurement on cold rolled and sensitized 304 specimens

Table 8: Results for EPR test on sensitized and cold rolled specimens

cold work [%]							
0	holding time [min]	0	10	30	60	120	180
	DOS [-]	1	2.66	1.47	9.37	12.32	16.6
7	DOS [-]	1	1.12	5.15	24.17	27.4	28
16	DOS [-]	1	7.96	26.62	91	204	190

7.5.1 Comparison of EPR and longitudinal results on 16% cold rolled specimen

Figure 36 illustrates the results of Figures 31 and 35 for the 16% cold rolled specimens. The left y-axis is correlated with the β measured longitudinal waves, whereas the right y-axis is related to the EPR results. This shows that sensitization is not detected

by longitudinal waves. As already mentioned the EPR test was made to confirm that sensitization is occurring in the 304 specimens and while the DOS is increasing over holding time, β has no visible changes, indicating that longitudinal waves are not sensitive to sensitization. Moreover this plot gives information about the susceptibility of cold rolled material proving that cold rolling is supporting sensitization, therefore weakening the material. The more sensitization, or the more chromium precipitates at the grain boundaries, the more susceptible the material gets to stress corrosion cracking.

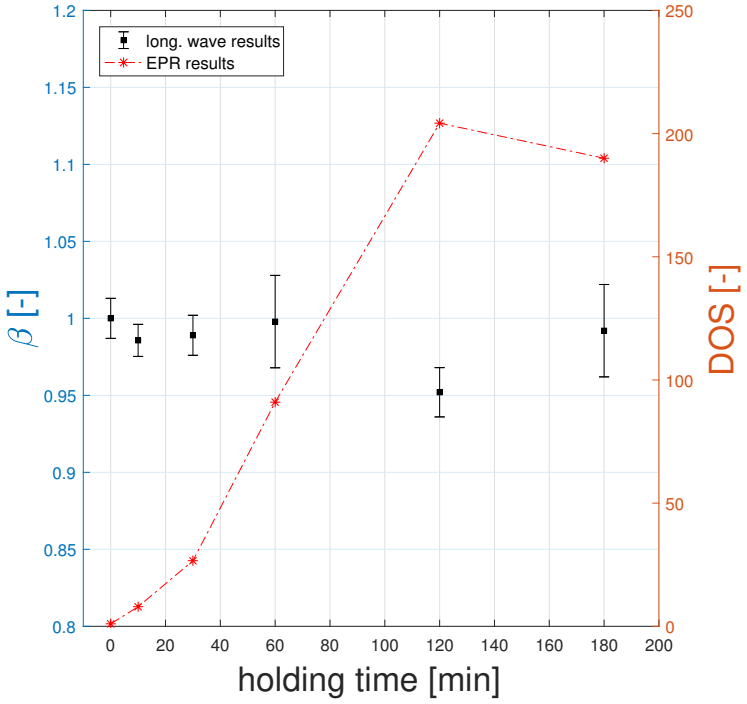

Figure 36: Results for the EPR and longitudinal wave measurument in contrastfor 16% cold rolled 304 SS

CHAPTER VIII

CONCLUSION AND OUTLOOK

8.1 Conclusion

This research used nonlinear ultrasonic waves and electrochemical potentiodynamic reactivation (EPR) to detect chromium carbide precipitation and the effect of grain deformation due to cold rolling and sensitization in 304 SS specimens. For the ultrasonic measurement methods the first and second harmonic waves in the material was measured and the nonlinearity parameter, β, was calculated, giving information about the microstructural changes. The EPR test measured the absolute degree of sensitization by measuring the change of current of the electrodes. Two ultrasonic wave methods were used: Rayleigh waves that are propagating along the surface of the specimens and longitudinal waves propagating through the thickness.

The Rayleigh wave measurement showed that Rayleigh waves are sensitive to cold work and that β increases, the more cold work is present in the material. The same result was seen by the longitudinal measurements and even the increase of β only differed minimally to the Rayleigh results. Comparing the results for the Rayleigh and longitudinal measurements on cold rolled 304 SS it can be seen that the nonlinearity parameter nearly experiences the same increase with the same amount of cold work in the material, proving that both methods are sensitive to cold work.

The results for cold rolled and then sensitized 304 SS specimens were different. Sensitization had no visible effect on β when measured by longitudinal waves resulting in no change of the parameter for different holding times, neither for previously cold rolled, nor unprepared specimens. This lead to the conclusion that longitudinal waves are sensitive to cold work, but not sensitization of 304 SS.

This statement is supported by a comparison of a sensitized specimen that was measured with both ultrasonic methods. Whereas β is experiencing an increase for the Rayleigh measurement that is comparable to previous work, the longitudinal measurement can not detect any changes.

Previous work showed that sensitization is weakening cold rolled 304 SS more, than an unrolled specimen. The EPR test showed that DOS is increasing more for cold rolled specimens compared to an unrolled specimen. This means, cold rolling beforehand sensitization is accelerating the sensitization effect. This could be by the deformation of the grains due to cold work, leaving more room between the grains and therefore is making it easier for the chromium to precipitate. This result is also comparable to previous research. This leads to the conclusion that the more sensitization is occurring in the material, the more susceptible it gets to IGSCC and that cold rolling before sensitization is accelerating the formation of microcracks.

Removing the undulated surface of the specimen after cold rolling by surface grinding caused β to vary for the Rayleigh waves and no predictable trend can be seen. Comparing this with the results where the surface was measured after cold rolling without post preparation leads to the fact that due to the surface grinding, the cold worked layer was taken off accidentally. This would mean that cold work transformation starts at the surface layers and then passes through the thickness with every thickness reduction step. However, this theory has to be proven by microstructural analysis first.

8.2 Outlook

This research provides results for the sensitivity of nonlinear ultrasonic waves on cold rolled and sensitized 304 SS. However, it has to be clarified why longitudinal waves are not sensitive to sensitization. By investigating on the microstructure after every sensitization step, more assumptions could be made on the grain deformation,

chromium precipitation and also the deformation induced martensite. Moreover, the Rayleigh wave measurement setup has to be improved. The clamping forces for the wedge and coupling conditions are not ideal. This could be changed by using pressure sensors and a better apparatus setup. To get the best results for both, Rayleigh and longitudinal measurements, the cold rolling process has to be elaborated. The biggest problem for this research was the wavy surface that the cold rolling process caused on the specimens. Bending and waves on the surface have to be suppressed to achieve the best results, since nonlinear ultrasonic measurements are highly dependent on surface conditions. Another point worth investigating on is the influence of annealing. It is assumed that due to oxidization, the nonlinearity parameter increases after annealing out the cold work. It is nevertheless unsure if that was just the result of bad surface conditions, or a composition change inside the material.

APPENDIX A

ANNEALED SPECIMENS

A.1 Results for longitudinal wave measurement on cold rolled and annealed 304 stainless steel specimen

This research is also focusing on the effect of annealing on 304 SS. Doerr [5] showed that annealing and water quenching beforehand thermical treatment makes the material more homogeneous and putting the specimens on the same "baseline". This means that previous processing of the material, either thermical or mechanical, is removed due to the annealing process. A specimen was taken, annealed at 1080°C, then cold rolled up to 16% thickness reduction and another annealing after that. During the processing steps, longitudinal wave measurements were taken and the surface was hand polished with sand paper GRIT 2500.

Figure 37 illustrates the results for β normalized to the results taken after the first annealing. As seen before, the measurement procedure is sensitive to cold rolling changes in the material, causing β to increase up to 50%. Surprisingly, β is still increasing after the last annealing step, whereas it was supposed to drop to nearly the origin again. This increase could be due to bad surface conditions after the last annealing step. Annealing affects the surface tremendously, leaving small visible pits after hand polishing. Those pits change the coupling conditions between transducers and surface, resulting in an increase of β.

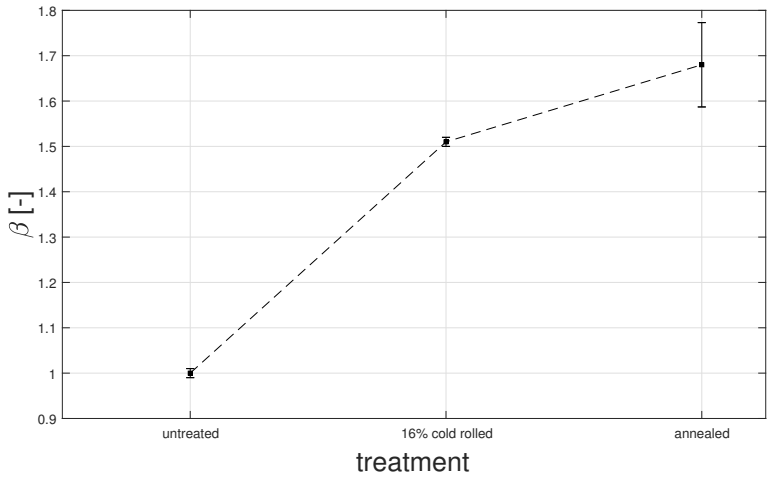

Figure 37: Results for cold rolled, then annealed 304 ss specimen

Figure 38 illustrates the effect of annealing 304 SS after it was already cold rolled. As it can be seen,β increases after the material is being cold rolled and is drastically reduced by the post annealing process. Strangely, the increase of β from unrolled to 16% cold rolled is too drastic and cannot be explained completely.

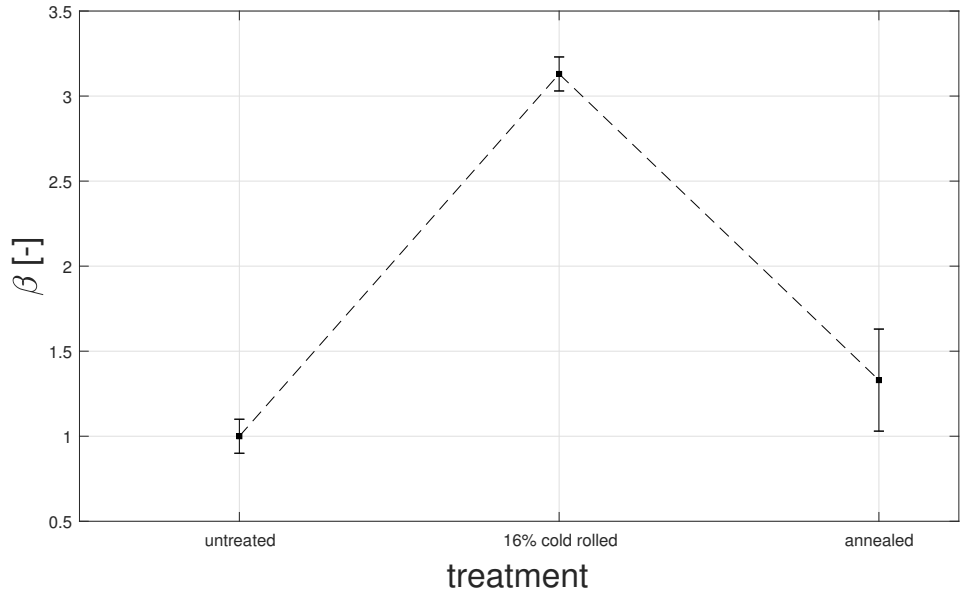

Figure 38: Results for the longitudinal wave measurement on annealed, cold rolled and annealed again, specimens

REFERENCES

[1] Achenbach, J., *Wave Propagation in Elastic Solids*. North-Holland Publishing Company/American Elsevier, 1973.

[2] ASTM, "G108-94 standard test method for electrochemical potentiodynamic reactivation (eprexample)," 2015.

[3] Beltran, R., Maldonado, J., Murr, L., and Fisher, W., "Effects of strain and grain size on carbide precipitation and corrosion sensitization behavior in 304 stainless steel," *Acta Materialia*, vol. 45, no. 10, pp. 4351 – 4360, 1997.

[4] Blackstock, D. T. and Hamilton, M. F., *Nonlinear acoustics*. Acoustical Society of America, 2008.

[5] Doerr, C., "Evaluation of sensitization in aisi 304 and aisi 304l stainless steel with nonlinear ultrasonic rayleigh wave measurements," Master's thesis, Georgia Institute of Technology, Atlanta, GA, USA, 8 2016.

[6] Doerr, C., Kim, J.-Y., Singh, P., Wall, J. J., and Jacobs, L. J., "Evaluation of sensitization in stainless steel 304 and 304l using nonlinear rayleigh waves," *NDT & E International*, vol. 88, pp. 17 – 23, 2017.

[7] Graff, K. F., *Wave Motion in Elastic Solids (Dover Books on Physics)*. Dover Publications, June 1991.

[8] Herrmann, J., Kim, J.-Y., Jacobs, L. J., Qu, J., Littles, J. W., and Savage, M. F., "Assessment of material damage in a nickel-base superalloy using nonlinear rayleigh surface waves," *Journal of Applied Physics*, vol. 99, no. 12, p. 124913, 2006.

[9] Kim, J.-Y., Jacobs, L. J., Qu, J., and Littles, J. W., "Experimental characterization of fatigue damage in a nickel-base superalloy using nonlinear ultrasonic waves," *The Journal of the Acoustical Society of America*, vol. 120, no. 3, pp. 1266–1273, 2006.

[10] Kocsisova, E., Domankova, M., Slatkovsky, M., and Sahul, M., "Study of the sensitization on the grain boundary in austenitic stainless steeil aisi 316," *FACULTY OF MATERIALS SCIENCE AND TECHNOLOGY IN TRNAVA*, vol. 2, no. Special number, pp. 131–136, 2014.

[11] Matlack, K. H., Wall, J. J., Kim, J.-Y., Qu, J., Jacobs, L. J., and Viehrig, H.-W., "Evaluation of radiation damage using nonlinear ultrasound," *Journal of Applied Physics*, vol. 111, no. 5, p. 054911, 2012.

[12] Mumtaz, K., Takahashi, S., Echigoya, J., Kamada, Y., Zhang, L. F., Kikuchi, H., Ara, K., and Sato, M., "Magnetic measurements of martensitic transformation in austenitic stainless steel after room temperature rolling," *Journal of Materials Science*, vol. 39, pp. 85–97, Jan 2004.

[13] nCode, "HAZ." `http://www.ncode.com/en/solutions/fatigue-analysis-of-seam-welds/`. [Online; accessed 13-June-2017].

[14] Railway Fasteners, "Work Hardening." `http://www.railway-fasteners.com/news/processes-of-rail-components-comparison.html`, unknown. [Online; accessed 13-June-2017].

[15] Schino, A. D., Salvatori, I., and Kenny, J. M., "Effects of martensite formation and austenite reversion on grain refining of aisi 304 stainless steel," *Journal of Materials Science*, vol. 37, no. 21, pp. 4561–4565, 2002.

[16] Scott, K., Kim, J.-Y., Wall, J. J., Park, D.-G., and Jacobs, L. J., "Investigation of fe-1.0nonlinear ultrasound," *NDT & E International*, vol. 89, pp. 40 – 43, 2017.

[17] Singh, R., Chattoraj, I., Kumar, A., Ravikumar, B., and Dey, P. K., "The effects of cold working on sensitization and intergranular corrosion behavior of aisi 304 stainless steel," *Metallurgical and Materials Transactions A*, vol. 34, no. 11, pp. 2441–2447, 2003.

[18] Thiele, S., Kim, J.-Y., Qu, J., and Jacobs, L. J., "Air-coupled detection of nonlinear rayleigh surface waves to assess material nonlinearity," *Ultrasonics*, vol. 54, no. 6, pp. 1470 – 1475, 2014.

[19] Trillo, E., Beltran, R., Maldonado, J., Romero, R., Murr, L., Fisher, W., and Advani, A., "Combined effects of deformation (strain and strain state), grain size, and carbon content on carbide precipitation and corrosion sensitization in 304 stainless steel," *Materials Characterization*, vol. 35, no. 2, pp. 99 – 112, 1995.

[20] Viswanath, A., Rao, B. P. C., Mahadevan, S., Parameswaran, P., Jayakumar, T., and Raj, B., "Nondestructive assessment of tensile properties of cold worked {AISI} type 304 stainless steel using nonlinear ultrasonic technique," *Journal of Materials Processing Technology*, vol. 211, no. 3, pp. 538 – 544, 2011.